Population genomics of the muskox' resilience in the near absence of genetic variation

Patrícia Pečnerová[1,2,*], Edana Lord[3,4,5], Genís Garcia-Erill[1], Kristian Hanghøj[1], Malthe Sebro Rasmussen[1], Jonas Meisner[1], Xiaodong Liu[1], Tom van der Valk[3,4], Cindy Gilda Santander[1], Liam Quinn[1,6], Long Lin[1], Shanlin Liu[7,8], Christian Carøe[8], Fredrik Dalerum[5,9,10], Anders Götherström[3,11], Johannes Måsviken[3,4,5], Sergey Vartanyan[12], Katrine Raundrup[13], Amal Al-Chaer[1], Linett Rasmussen[2,8], Christina Hvilsom[2], Mads Peter Heide-Jørgensen[13,14], Mikkel-Holger S. Sinding[1,13], Peter Aastrup[15,16], Peter J. Van Coeverden de Groot[17], Niels Martin Schmidt[15,16], Anders Albrechtsen[1], Love Dalén[3,4,5], Rasmus Heller[1], Ida Moltke[1], Hans Redlef Siegismund[1]

1. Section for Computational and RNA Biology, Department of Biology, University of Copenhagen, Ole Maaløes Vej 5, DK-2200 Copenhagen N, Denmark
2. Copenhagen Zoo, Roskildevej 38, DK-2000 Frederiksberg, Denmark
3. Centre for Palaeogenetics, Svante Arrhenius väg 20C, SE-106 91 Stockholm, Sweden
4. Department of Bioinformatics and Genetics, Swedish Museum of Natural History, P. O. Box 50007, SE-104 05 Stockholm, Sweden
5. Department of Zoology, Stockholm University, SE-106 91 Stockholm, Sweden
6. Department of Clinical Immunology, Zealand University Hospital, Køge, Denmark
7. Department of Entomology, College of Plant Protection, China Agricultural University, Beijing 100193, China
8. The GLOBE Institute, Faculty of Health and Medical Sciences, University of Copenhagen, Øster Voldgade 5-7, DK-1350 Copenhagen K, Denmark
9. Biodiversity Research Institute (UO-CSIC-PA), Spanish National Research Council, Mieres Campus, E-33600 Mieres, Spain
10. Mammal Research Institute, Department of Zoology and Entomology, University of Pretoria, Private Bag x 20, 0028 Hatfield, South Africa
11. Archaeological Research Laboratory, Department of Archaeology and Classical Studies, Stockholm University, Wallenberglaboratoriet, SE-106 91 Stockholm, Sweden
12. North-East Interdisciplinary Scientific Research Institute N.A.N.A. Shilo, Far East Branch, Russian Academy of Sciences, 68500 Magadan, Russia
13. Greenland Institute of Natural Resources, 3900, Nuuk, Greenland
14. Greenland Institute of Natural Resources, Strandgade 91, DK-1401 Copenhagen, Denmark
15. Department of Ecoscience, Aarhus University, 4000 Roskilde, Denmark
16. Arctic Research Centre, Aarhus University, 8000 Aarhus, Denmark
17. Department of Biology, Queen's University, Kingston, ON R3L 1K3, Canada
*Corresponding author: pata.pecnerova@gmail.com

Abstract

Genomic studies of species threatened by extinction are providing crucial information about evolutionary mechanisms and genetic consequences of population declines and bottlenecks. However, to understand how species avoid the extinction vortex, insights can be drawn by studying species that thrive despite past declines. Here, we studied the population genomics of the muskox (*Ovibos moschatus*), an Ice Age relict that was at the brink of extinction for thousands of years at the end of the Pleistocene yet appears to be thriving today. We analyzed 108 whole genomes, including present-day individuals representing the current native range of both muskox subspecies, the white-faced and the barren-ground muskox (*O. moschatus wardi* and *O. moschatus moschatus*), as well as a ~21,000-year-old ancient individual from Siberia. We found that the muskox' demographic history was profoundly shaped by past climate changes and post-glacial recolonizations. In particular, the white-faced muskox has the lowest genome-wide heterozygosity recorded in an ungulate. Yet, there is no evidence of inbreeding depression in native muskox populations. We hypothesize that this can be explained by the effect of long-term gradual population declines that allowed for purging of strongly deleterious mutations. This study provides insights into how species with a history of population bottlenecks, small population sizes, and low genetic diversity survive against all odds.

Keywords

Introduction

Due to habitat loss and other anthropogenic impacts, many species worldwide are experiencing declining population trends (Pimm & Raven, 2000; Powers & Jetz, 2019). Once a population becomes small, it is more likely to become extinct due to stochastic factors including environmental and demographic changes, natural catastrophes, as well as genetic factors (Caughley, 1994; Lande, 1993; Shaffer, 1981). Studying genetic extinction factors in wild populations has been facilitated by the developments in high-throughput sequencing, and in recent years, a lot of effort in wildlife genetics and ancient DNA research has focused on investigating the genetic consequences of population declines (Díez-del-Molino et al., 2018; Primmer, 2009; Steiner et al., 2013).

Inbreeding depression induced by low genetic diversity in small populations is a major concern as a genetic extinction factor (Caughley, 1994). Evidence of inbreeding depression has been documented in a number of genomic studies in wild populations, including the Soay sheep (Stoffel et al., 2021), Arctic fox (Hasselgren et al., 2021), and the Isle Royale wolves (Robinson et al., 2019). On the other hand, small populations can sometimes persist without any evidence of inbreeding depression, which was observed in the mountain gorillas (Xue et al., 2015), Channel Island foxes (Robinson et al., 2016, 2018), Tasmanian devils (Gooley et al., 2017), and vaquita (Morin et al., 2021), among other taxa. It has been hypothesized that this survival is facilitated by purging of strongly deleterious mutations in small populations and that it depends on the pace of the population decline (Kyriazis et al., 2021, 2022; Robinson et al., 2019; van der Valk et al., 2021). However, it remains unclear how such mechanisms operate, and under which conditions they become effective.

An understanding of the genomic processes that accompany a population decline requires analyzing a diverse range of study systems and scenarios. To date, studies have focused on genomic analyses of endangered populations that have experienced recent (Dussex et al., 2021; van der Valk et al., 2019) or ancient (Robinson et al., 2016; Xue et al., 2015) bottlenecks, and the pre-extinction processes in an extinct species using ancient DNA (Pečnerová et al., 2016; Pečnerová, Palkopoulou, et al., 2017; Thomas et al., 2019). However, most of this research is based on populations that have few individuals, are geographically restricted, or are carnivores at the top of the trophic pyramid that typically have low population sizes. Few studies so far have investigated populations that have experienced considerable population declines, yet appear to be thriving today.

In this study, we explore the population genomics of an Ice Age relict, the muskox (*Ovibos moschatus*). The muskox is an Arctic tundra specialist, physiologically and behaviorally adapted to living in the cold conditions of the highest latitudes. While its Pleistocene distribution spanned across the Holarctic, the muskox' current native range is restricted to northern Canada and Greenland (Canteri et al., 2022; Cuyler et al., 2020). Two subspecies are commonly recognized, the barren-ground muskox (*O. moschatus moschatus*) on the Canadian mainland and the white-faced muskox (*O. moschatus wardi*) in the Canadian Islands and in Greenland (Van Coeverden de Groot, 2001; Hansen et al., 2018). Along with many other Ice Age megafauna species, the muskox suffered reductions in population size and range as the climate and environment changed at the end of Pleistocene (Campos et al., 2010; Canteri et al., 2022). However, unlike woolly mammoths, steppe bison, and other steppe tundra herbivores, the muskox still survives today.

Currently, the muskox' is not considered directly threatened by extinction according to the IUCN Red List (Gunn & Forchhammer, 2022), and despite varying regional population trends, the species numbers ca 170,000 individuals globally (Cuyler et al., 2020).

Nevertheless, the demographic history of the muskox is characterized by population reductions and expansions, which has left a strong imprint on its genetic makeup (Campos et al., 2010; Groves, 1997; Hansen et al., 2018; Prewer et al., 2020). The muskox is reported to have extremely low genomic diversity, particularly in the areas that they colonized most recently, such as East Greenland (Hansen et al., 2018). Despite this, there is no evidence of inbreeding depression in the native muskox populations or in the reintroduced West Greenland population, which experienced exponential growth after being founded by 27 translocated individuals (Cuyler et al., 2020; Hansen et al., 2018; Olesen, 1993). Thus, the muskox represents an interesting case study on how a large herbivore with a documented history of population bottlenecks and low genetic variation has avoided the extinction vortex thus far.

The muskox is a key species of the tundra ecosystem, impacting plant communities (Mosbacher et al., 2019), nutrient translocation (Mosbacher et al., 2016), and its grazing may to some extent buffer the ecosystem changes related to the warming Arctic (Falk et al., 2015). Understanding how the largest Arctic herbivore is faring is thus of importance for predicting the future of Arctic ecosystems. We used whole-genome data from a ~21,000 year old muskox from Siberia and 107 modern muskoxen from Canada and Greenland, and investigated the evolutionary history of the muskox to understand the context of its extremely low genetic diversity. This study aimed to provide new insights into how the muskox survives and thrives against all odds.

Results

Dataset

We re-sequenced an ancient genome of a muskox from Wrangel Island, Siberia, radiocarbon-dated to 21,395 cal BP, and whole genomes of 178 present-day muskoxen from Canada and Greenland, representing the stronghold of their current native range (Figure 1; Table S1; Figure S1). Out of the 178 modern muskox genomes sequenced, only 107 passed our sample quality filters. Samples were excluded due to poor preservation of opportunistically collected samples, species misidentification, and sample duplication (see Methods for details).

The 107 modern genomes were sequenced to 1-28X genomic coverage and mapped both to a muskox reference genome generated as part of this study (see Methods for details) and the sheep reference genome (Oar_rambouillet_v1.0 - GCF_002742125.1). After filtering the reference genomes for scaffold size, sex-linked scaffolds, repetitive regions, mappability, excess heterozygosity, and extreme depth, the number of resulting genomic sites used in the downstream analyses was 1,211,258,554 for the dataset mapped to the muskox reference and 814,035,139 for the dataset mapped to the sheep reference (Table S2). For analyses requiring high-depth data, we used a subset of the samples (60 modern and 1 ancient) that had at least 9.5X depth of coverage (Table S10), and for the dataset including low-depth data we performed analyses based on genotype-likelihoods and single-read sampling (Table S12).

Population structure

A Neighbor-Joining (NJ) tree (Saitou & Nei, 1987) of genetic distances based on an IBS matrix (Korneliussen et al., 2014) identified three main groupings – the ancient Siberian muskox (SIB), the barren-ground muskox including the Canadian mainland West (CaMW) and East (CaME), and the white-faced muskox including the Canadian islands South (CaIS) and North (CaIN), Greenland North (GrN), and Greenland East-North (GrEN) and East-South (GrES) (Figure 2A).

4

In a principal component analysis (PCA) performed with PCAngsd using genotype-likelihoods (Meisner & Albrechtsen, 2018), the modern samples were separated into three main clusters on the first two principal components, representing the Canadian mainland (CaM), Canadian islands (CaI), and Greenland (Gr) (Figure S2, Figure S3). Within Greenland, there was a separation between North (GrN) and the two eastern populations (GrEN and GrES). Interestingly, the first principal component, which separates the two subspecies of muskox, captures 75.44% of the variation in the data. On the subsequent principal components (Figure S2), we found splits within mainland Canada (West and East: CaMW and CaME) and within the Canadian islands (South and North: CaIS and CaIN). However, within some of the clusters (particularly CaME, CaIS, and CaIN), we observed continuous clines in the genetic variation, suggesting that these are not completely isolated units. The ancient Siberian muskox (SIB) was positioned in the middle between the three groups. As a single sample without contemporaneous representation, its position in the PCA might be biased, but a PCA based on the sheep-mapped data supports this placement.

The structure observed on the first four principal components mirrors that observed when estimating admixture proportions using ngsAdmix (Skotte et al., 2013). At K=6 (Figure 2C), we identify clusters that broadly correspond to the geographical regions the samples are from: West and East Canadian mainland (CaMW and CaME), South and North Canadian islands (CaIS and CaIN), as well as Greenland East-North (GrEN) and East-South (GrES). Greenland North (GrN) and SIB are modeled as a mixture of ancestries, but this observation is likely the consequence of analyzing singleton samples (Figure S4). We ran the ngsAdmix analysis modeling up to 13 clusters, however at K=9-13 the analysis did not converge. We considered clustering into six ancestry components as the best fit to the data, since at K=7 and K=8 (Figure S4) the analyses picked up substructure within the East Canadian mainland (CaME) and North Canadian islands (CaIN), which is difficult to interpret biologically. Evaluation of the model fit in evalAdmix (Garcia-Erill & Albrechtsen, 2020) confirmed the presence of correlated residuals within those two locations as well as in GrES, which is evidence of unresolved substructure, even at K=8 (Figure S5).

We tested our population groupings both at geographic region and sampling location level using *D*-statistics (ABBA-BABA) (Durand et al., 2011; Green et al., 2010) by evaluating the affinity of pairs of samples within each region/location (P1 and P2), compared to a sample from another region/location (P3), using the sheep as an outgroup (P4). All groups showed sub-structuring (Figure S6, Figure S7), particularly with geographically close locations, which suggests that there is some gene flow between them. This is consistent with the continuous structure observed within certain clusters in the PCA (Figure S2), the observed correlated residuals from the estimated admixture proportions, as well as the fact that the genetic clustering deviates from the pattern expected based on geography in some populations. In particular, there are two locations that considerably deviate from the pattern expected based on geography. The location Fort Ross (FR) is on a peninsula connected to the Canadian mainland, but in terms of physical distance was assumed to be connected to CaIS. Yet, the structure analyses place it into the region CaIN (Figure 2A, 2C, S2). Even more interestingly, the location Cornwallis Island (CI) includes two samples that cluster together with CaIS and two samples that cluster with CaIN (Figure 2A, 2C, S2). These new findings were incorporated into our final group identifications and in the plots (Figure 2) are shown with the adjusted groupings.

Next, we quantified the extent of population differentiation between the geographic regions with the fixation index F_{ST} using two methods, which complement each other at overcoming some limitations of our data. A per-individual approach is less affected by population

5

structure and uncertainty in reliably defining populations, and allows regions from which there is only one sample (SIB and GrN) to be included in the analyses. In contrast, a per-population approach gains information from multiple samples and is not influenced by inbreeding. Both methods yielded very similar results and the estimated F_{ST} values showed extremely high levels of differentiation between the present-day muskox populations (Table S3). The highest F_{ST} (0.80 per individual and 0.76 per population) was observed between the two most geographically distant regions of West Canadian mainland and East-South Greenland. The lowest F_{ST} values were between the West and East Canadian mainland (0.21 per individual and 0.15 per population). Interestingly, the F_{ST} between the two regions in East Greenland (GrEN and GrES) was higher (0.69) than that of each of the populations compared to the North Greenland population (0.36 and 0.51 for GrEN and GrES, respectively). The differentiation between the ancient Siberian sample (SIB) and the modern-day populations was lower than the differentiation between most of the groups, consistent with genetic drift driving the differentiation of modern populations since the split from the common ancestor.

We visualized the levels of genetic connectivity by estimating migration rates with EEMS (Petkova et al., 2016), which identified barriers to gene flow consistent with the identified patterns of structure (Figure 2B). Overall, samples cluster into the preliminary groupings proposed based on geography (Figure 1); however, substructure and gene flow seem to prevent the samples from forming homogeneous genetic units.

Population history

To explore how these complex patterns of population structure and gene flow originated, we analyzed the phylogenetic relationships of the muskox populations. Firstly, we constructed a mitochondrial phylogeny using reads that mapped to the mitochondrial part of the merged nuclear-mitochondrial muskox reference. Competitive mapping to both the nuclear and mitochondrial genome should result in preferential mapping of NuMts (Kolokotronis et al., 2007) to their nuclear sites (Marshall & Parson, 2021), consistent with the lowered number of reads compared to direct mapping to the mitogenome observed here.

In contrast to the relationships inferred by the nuclear NJ tree, the mitochondrial phylogeny identified a highly divergent, but well-supported clade among the Canadian mainland samples (Figure S8, Figure S9, Figure S10, Figure S11). To investigate this discrepancy further we combined our data with mtDNA from previous studies of ancient samples (Campos et al., 2010) and observed that the samples of the divergent clade cluster outside of the diversity of present-day muskoxen, and instead cluster together with a clade comprising a Canadian sample from Herschel Island dated to 1,005 calBP and Siberian samples from Taimyr dating to ~19,000-3,000 calBP. Based on the molecular dating, the most recent common ancestor of these two mitochondrial clades is ~60 kya (95% HPD: 68,653-54,592 ya). Excluding the divergent clade, the modern muskoxen in our dataset have a most recent common ancestor between ~19-10 kya. For the Greenlandic muskoxen, the divergence of the Greenland East-North samples (GrEN) occurred 3,436 ya (95% HPD: 5,951-1,711 ya) and of the Greenland East-South samples 1,953 ya (95% HPD: 3,968-479 ya).

To investigate whether the discordance between the nuclear and mitochondrial trees is a result of gene flow, we used *D*-statistics (Durand et al., 2011; Green et al., 2010), TreeMix (Pickrell & Pritchard, 2012), and qpGraph (Patterson et al., 2012). All of these analyses were performed with the sheep-mapped dataset to remove reference bias, and with the sheep as an outgroup. In the *D*-statistics analyses we specified the ancient Siberian genome as P3, and all pairs of modern populations in P1 and P2 (Figure S12). The results, which were based on

called genotypes in high-depth samples, suggest that all modern populations are equally distant to the ancient Siberian genome. Consistent with this our TreeMix results placed the ancient Siberian genome as an outgroup to all the modern populations (Figure 2D). The TreeMix results also show that a model with two migration edges was selected as the best fit to the data (Figure 2D, Figure S13). These migration edges suggest gene flow from the West Canadian mainland (CaMW) to South Canadian islands (CaIS), and from North Canadian islands (CaIN) to North Greenland (GrN). The best fitting admixture graph from qpGraph also placed the ancient Siberian sample as an outgroup to all modern muskox populations (Figure 2E), and had no significantly deviating residual f-statistics (Figure S14). In accordance with TreeMix, the best fit is with migration from the CaMW to the Canadian island populations. While qpGraph did not support admixture from CaIN to GrN, CaIN had a higher amount of ancestry from the lineage shared with Greenland than CaIS.

Demographic history and genetic diversity
To better understand the observed patterns of genetic variation, we reconstructed the muskox' demographic history (Figure 3). However, the nature of our data revealed some limitations of the PSMC analysis (Li & Durbin, 2011) in conditions of very low variation. PSMC estimates the most recent common ancestor in a window-based approach determined by the density of heterozygous sites. In populations that have experienced strong bottlenecks, there are too few coalescence events in the deeper past for a reliable inference (Foote et al., 2023). We removed the Greenlandic populations from the analysis as these showed trajectories that were difficult to explain biologically, likely due to the extremely low levels of heterozygosity (Figure S15). Despite this, the Canadian muskoxen showed a very consistent pattern, with the differences in individual trajectories due to differing levels of heterozygosity. Muskox experienced a population decline from 1-2 million years ago (mya) until 500 thousand years ago (kya). After that, there was a period of stable effective population size until approximately 30 kya, which marked the onset of a second population decline until 10-5 kya. At 5 kya, the muskox' effective population size was ~300 in the island populations and ~500 on the mainland, and subsequently remained low. We also used PopSizeABC (Boitard et al.,2016) on muskox populations using data mapped to the sheep reference genome to estimate changes in population sizes at more recent time points in history where PSMC has less resolution (i.e. less than 20,000 years ago till present). Results from the four populations that were analysed (Figure S16) all show a common population bottleneck approximately 10,000 ya consistent with PSMC. After the bottleneck all populations experienced a population recovery until 200-300 ya where all population sizes remained at a stable level to present day. Due to small sample sizes and the low variation affecting resolution, we refrain from interpreting the regional differences in the timing and scale of the population size change.

To study how population history and population structure have affected genetic diversity, we estimated genome-wide heterozygosity. Three different ways of estimating heterozygosity yielded very consistent results (Table S4). We observed a ~3- to 14-fold decrease in diversity between the ancient Siberian genome ($H_O = 8.3 \times 10^{-4}$) and the barren-ground ($H_O = 2.6 \times 10^{-4}$) and white-faced ($H_O = 0.6E-4$) muskox, respectively (Figure 4A, Figure 5, Figure S17, Figure S18, Table S4). Within the Canadian islands, there was a gradual decline of diversity from the west towards the east. Remarkably, the East-South Greenland population (GrES) had an extremely low heterozygosity based on genotype likelihoods ($H_O = 0.23 \times 10^{-4}$ - 0.37×10^{-4}) and called genotypes in a subset of high coverage samples ($H_O = 0.083 \times 10^{-4}$ - 0.1773×10^{-4}), the lowest of which translates to ~2 variable sites per 100kb (Table S4). The extremely homozygous estimates in GrES and GrEN also revealed a limitation of the ROHan analysis,

which cannot estimate heterozygosity below 0.8×10^{-4}, and the heterozygosity of all individuals from these regions was thus capped at this value. The ROH analyses identified high inbreeding coefficients (F_{ROH}) and that a large proportion of the genome is depleted of variation (Figure 4B, 6, Figure S19, Table S5, Table S6). Both proportion (Figure 4B) and size of ROH (Figure S19) generally increase from the Canadian mainland to the East Greenland. The East Greenland populations showed extremely high F_{ROH} (>1MB) of on average 77% in PLINK or 90% in ROHan (Chang et al., 2015; Purcell & Chang, 2015). Particularly the GrEN population had a large proportion of very large ROH, including above 10 MB. Since the estimates might be influenced by the parameters set in PLINK and the quality of the reference genome, which is resolved only to scaffold-level, we note that the length-distribution estimates should be interpreted with care.

Genetic load

To understand the impact of low genomic diversity and sustained low population size, we estimated mutational load across the populations based on evolutionary conservation in a multi-species alignment (Bertorelle et al., 2022). We estimated the relative mutational load, i.e. the average genomic evolutionary rate profiling (GERP) score of derived alleles in regions across the genome estimated with GERP++ v2.1 (Davydov et al., 2010; Kutschera et al., 2022; van der Valk et al., 2021). Consistent with originating from a larger population, the Siberian sample exhibits the highest relative mutational load of all the samples analyzed (Figure 4C, Figure S20, Table S8). Accordingly, the barren-ground muskox shows higher relative mutational load than the white-faced muskox.

Second, we estimated the mutational load based on functional annotation from snpEff (Cingolani et al., 2012) by predicting putative deleterious variation in four impact categories: high impact (loss of function), moderate impact (missense), low impact (synonymous), and modifier (non-coding). Based on the functional annotation, we estimated mutational load in three ways. First, we report the total load as the number of derived alleles at sites from a certain impact category out of 100,000 derived alleles (Figure 7, Figure S21, Figure S22). Second, we report the potential load, which is the fraction of an individual's genotypes with at least one derived allele that has a certain impact annotation (Figure S23, Table S9). Third, we report the (recessive) realized load, the fraction of homozygous derived genotypes within a certain impact category (Figure S23, Table S9). In the total and potential load estimates, the ancient Siberian muskox genome had a higher proportion of deleterious alleles in the high and moderate impact categories. In the realized load, the ancient Siberian genome had lower load then the modern genomes, consistent with the higher homozygosity of the modern populations. It should be noted that the ancient genome had overall slightly more derived alleles than the modern genomes (on average 0.26%), but compared to the non-coding category of modifier mutations, where the ancient Siberian genome also has 0.26% more derived alleles, the stronger impact categories show an additional excess of derived alleles, averaging 0.63% in the moderate impact category and 2.43% in the high impact category. We further describe the steps taken to ensure that the modern and ancient genomes are comparable in the Method section *Reliability of the ancient-modern sample comparisons*, and we suggest the genetic load analyzes to be interpreted with care.

Discussion

The muskox occupied diverse habitats in the Pleistocene ecosystem, which might have allowed it to persist through periods of less favorable environmental conditions, as well as maintain connectivity across sub-optimal habitats (Lent, 1998). This also likely facilitated the muskox' recolonization of circumpolar tundra after the Last Glacial Maximum (LGM) and its survival until present (Kahlke, 2014), in contrast to many other Ice Age megafauna species that became extinct towards the end of the Late Pleistocene (Lorenzen et al., 2011).

The ability to survive climatic changes and unfavorable environmental conditions made the muskox well adapted to the Arctic tundra, which is reflected in the stable effective population sizes over most of the Pleistocene (Figure 6), and contrasts with population declines or expansion observed in other Ice Age megafauna in association with previous glacial-interglacial cycles (Lord et al., 2020; Palkopoulou et al., 2015; Schubert et al., 2014). However, the muskox population size started to gradually decline ~30-20 kya, coinciding with the maximum extent of the Laurentide Ice Sheet (26-25 kya) during the Wisconsin glaciation (Stokes, 2017). In contrast to the stable population trend in earlier history, the Late Pleistocene and Holocene muskox demographic history was characterized by population fluctuations and founder events (Campos et al., 2010; Groves, 1997; Hansen et al., 2018; Tener, 1965), resulting in overall population decline until ~5 kya.

There has been an ongoing debate about the location of muskox refugia during the LGM (Groves, 1997; Hansen et al., 2018; Harington, 1961; Maher, 1968), when the Laurentide Ice Sheet covered most of present-day Canada and Greenland (Stokes, 2017). The phylogeographic data presented here show complex patterns and make interpretation of the results challenging. While the mitochondrial data (Figure S9, Figure S9, Figure S10) provide tentative information about the divergence times and location of the LGM refugia, the lack of power of the low-variation nuclear data does not allow for validation of these with more complex demographic models (as illustrated by the need to remove the most homozygous populations of GrEN and GrES from the qpGraph analysis). The accumulating genetic evidence thus suggests that the evolutionary history of the muskox and other Arctic mammals is defined by episodes of isolation and secondary contact (Dalén et al., 2005; Fedorov & Stenseth, 2002; Klütsch et al., 2017), resulting in complicated patterns of genetic drift and gene flow. We found clear signs of population structure (Figure 2) as shown by the clear separation into clusters in the PCA (Figure S2), strong barriers to gene flow in the EEMS analysis (Figure 2B), and the extremely high F_{ST} values (Table S3). However, we also found that these patterns were obscured by gene flow as suggested by the identification of individuals with mixed ancestry in ngsAdmix (Figure 2C), migration edges in TreeMix connecting the Canadian mainland with the islands, and northern islands with North Greenland (Figure 2D), the lack of well-defined groups in the population homogeneity analyses (Figure S6, Figure S7), and the fact that the high F_{ST} values are mainly driven by genetic drift rather than deep divergence. Moreover, population genomic analyses of the muskox are hindered by the lack of power due to the extremely low levels of genetic variation (Figure 4A, 6, Figure S17, Table S4), as illustrated by biased results in the most homozygous populations from East Greenland. This revealed that some analyses fall short under these conditions as described in the Results section '*Population history and genetic diversity*', e.g. ROHan (Table S5) and the PSMC (Figure S15), which is paradoxical since populations with depleted variation might be those where precise estimates are the most needed.

Extremely low levels of genetic variation in the muskox have been reported previously (Groves, 1997; Hansen et al., 2018; MacPhee et al., 2005; Prewer et al., 2020) and were here

confirmed by genome-wide estimates from across the species' range and through multiple analytical approaches (Figure 4A, Figure 5, Figure S17, Figure S18, Table S4). By including a 21,395 year old Siberian muskox, we find that even the populations that we consider relatively diverse today, still only have a third of the Late Pleistocene diversity (Figure 4A, Table S4). This observation is also consistent with the reduced mitochondrial haplotype diversity compared to past levels (Figure S9, Figure S10) (Campos et al., 2010).

The present-day levels of genetic diversity in Arctic taxa have been profoundly shaped by the Pleistocene glacial refugia and post-glacial recolonizations. The impact of glacial history has been documented in many of the terrestrial Arctic mammals, either using traditional genetic markers in e.g. collared lemmings (Fedorov & Stenseth, 2002), Arctic foxes (Dalén et al., 2005), and Arctic hares (Waltari & Cook, 2005), or more recently using genome-wide data, e.g. in grey wolves (Sinding et al., 2018), caribou (Taylor et al., 2021), and ermine (Colella et al., 2018). A reduction in population size during the LGM and early Holocene, as well as successive founder events during the recolonization of previously glaciated areas, led to the extremely low levels of genome-wide heterozygosity observed in present-day muskox. In fact, the muskox has the lowest diversity ever detected in a vertebrate herbivore (Figure 5), falling within the range of genome-wide heterozygosity values otherwise dominated by vertebrate predators. The vertebrate predators were traditionally associated with a higher risk of extinction due to the dependence on the lower trophic levels, slow life histories, and smaller population sizes that are associated with lower genetic diversity (Buffalo, 2021; Frankham, 1996; Purvis et al., 2000; Soule, 1976). However, a recent evaluation of extinction risks across trophic levels revealed that the highest proportion of threatened species is among herbivores (Atwood et al., 2020). This discrepancy corroborates previous findings that pointed out the lack of concordance between the level of genome-wide diversity and conservation status (Díez-del-Molino et al., 2018). Thus, the white-faced muskox of the Canadian Archipelago and Greenland, which numbers ~130,000 individuals (Cuyler et al., 2020) and is listed as "Least Concern" according to the IUCN Red List (Gunn & Forchhammer, 2022), has lower genome-wide heterozygosity than the "Critically Endangered" vaquita (Morin et al., 2021) and baiji (Zhou et al., 2013), or the "Endangered" Iberian lynx (Abascal et al., 2016) and Amur tiger (Cho et al., 2013). The only mammal taxon with a lower genetic variation than the white-faced muskox is the San Nicolas Island fox (Robinson et al., 2016). Some of the East Greenlandic muskoxen have lower genome-wide heterozygosity than those of the San Nicolas Island foxes. It is, however, possible that these estimates are biased by lower sequencing depth and strict filtering. Without using a standardized set of filtering criteria and analytical methods across all species, we note that these cross-species comparisons should be interpreted with caution.

Consistent with the low diversity, we observed very high rates of inbreeding in all modern muskox populations compared to the ancient Siberian muskox (Figure 4B, Table S5, Table S6), indicating that the high inbreeding is a legacy of the high fragmentation and isolation of the populations in the last 20,000 years. Although environmental shifts were the likely cause of muskox bottlenecks in the ancient past (Campos et al., 2010; Canteri et al., 2022), it does not exclude the role of humans in more recent times (Canteri et al., 2022). The muskox has been an important means of subsistence for people in the Arctic, including as the main food source of the Independence I culture people (Knuth, 1967). However, considerable declines are known from the late 1800s until the early 20th century due to intense hunting (Barr, 1991; Cuyler et al., 2020), leading to a near extinction of the species on the Canadian mainland (and potentially elsewhere) by 1917 (Barr, 1991). Unfortunately, without a denser temporal sampling, we cannot evaluate when, during the last 20,000 years, the decrease in

heterozygosity and increase in inbreeding occurred. However, it should be noted that the two populations with lowest inbreeding and highest heterozygosity in our dataset (Figure 4A) are those from the Thelon Basin area (TH and BL), which was recorded as having the highest abundance of muskox remaining by 1930 (Barr, 1991), as they were here protected from hunting (Cuyler et al., 2020).

Our results suggest that the relative mutational load and total load in sites with high and moderate impact is not elevated in all present-day populations compared to the ancient Siberian muskox (Figure 4C). This is consistent with the hypothesis that inbreeding led to purging of deleterious mutations from the gene pool, which might explain why there are no records of inbreeding depression in the present-day native muskox populations. While inbreeding depression has been observed as decreased fecundity and longevity in the Swedish population that originated by dispersal from a translocated Norwegian population (Laikre et al., 1997; Thulin et al., 2011), and it has been proposed as one of the potential causes of overgrown hooves in a translocated Kap Atholl population in Northwest Greenland (Mølgaard, 2002), there are no published reports of reduced fitness elsewhere, not even in the exponentially growing West Greenlandic population established by translocation from East Greenland (Olesen, 1993; Vibe, 1958).

Here, we can begin to hypothesize how the muskox survives despite the observed genomic erosion. The mounting evidence from genomic studies of wild populations suggests that the impact of low genomic diversity is related to the length and duration of a population decline. In species that experienced drastic declines from previously large population sizes, e.g. the baiji (Zhou et al., 2013) and the Grauer's gorilla (van der Valk et al., 2019), negative fitness consequences are of concern due to the potential fixation of harmful mutations, as has occurred in the Isle Royale wolves (Robinson et al., 2019). In contrast, species that experienced gradual population declines or long-term small effective population size seem unaffected by negative genomic consequences. This has been primarily described in endangered species that survive in small, fragmented and isolated populations like the mountain gorilla (van der Valk et al., 2019; Xue et al., 2015), vaquita (Morin et al., 2021), kakapo (Dussex et al., 2021), and the Ethiopian wolf (Mooney et al., 2023). Perhaps more surprisingly, historic declines and small population size have been also identified as key factors when explaining the extremely depleted genomic variation in species that today have relatively large census size and broad geographic distribution like the brown hyena (Westbury et al., 2018), the narwhal (Westbury et al., 2019), and here, the muskox.

It has been shown that long-term small effective population sizes can lead to purging of strongly deleterious mutations but accumulation of moderately and weakly deleterious mutations, as observed in e.g. the Channel Island foxes (Robinson et al., 2018), mountain gorillas (van der Valk et al., 2019), Alpine ibex (Grossen et al., 2020), and Indian tigers (Khan et al., 2021). While increased homozygosity caused by low effective population size, leading to purging of strongly deleterious recessive mutations seems to explain why these species still survive, the risk that the accumulation of milder-impact deleterious mutations poses in conjunction with generally high inbreeding in smaller populations is of concern for extant populations (Khan et al., 2021; Mathur & Andrew DeWoody, 2021). In contrast, the muskox, as well as the kakapo (Dussex et al., 2021) and Grauer's gorilla (van der Valk et al., 2019), also appear to show purging of moderately deleterious variation. In the kakapo study, this has been explained using forward simulations showing that in contrast to an extreme-bottleneck scenario, the gradual decline that occurred in the kakapo between 30,000 and 10,000 years ago, likely led to a slow increase in inbreeding, which provided substrate for

purifying selection to act even on milder-impact deleterious variation. The demographic history of kakapo on the Stewart Island and the resulting genetic load are strikingly similar to what we observe in the muskox. Thus, we hypothesize that the muskox has survived until present through the combined effect of gradual population decline and purging of strongly and moderately deleterious alleles from the gene pool due to long-term low population size.

Despite the above hypotheses for the survival of muskox, the genomic make up of this species is raising some concerns for its future. First, the estimates of effective population sizes (Figure 6) suggest that N_e remained low since it decreased to ~500 on the mainland and ~300 in the islands five thousand years ago. While these estimates should be considered with caution due to the inherent lack of robustness of PSMC in recent times, muskox N_e seems to have been at the lower limit of what is considered necessary for long term survival of a species (Franklin, 1980). Second, concerns are growing about the effect of climate change on the fine-tuned host-parasite systems in the Arctic, which is expected to result in increased emergence of diseases and infections in northern species (S. J. Kutz, 2004). Recent disease outbreaks in the muskox (S. Kutz et al., 2015; Tomaselli et al., 2016) and range expansions of muskox lungworm parasites (Kafle et al., 2020) are particularly concerning considering that the muskox' adaptive potential is likely compromised due to the extremely low levels of standing genetic variation. Third, the main threat to muskox survival is thought to be mild and humid winters with ice crusts and high snow cover that hinder the muskox' access to forage (Desforges et al., 2021; Schmidt et al., 2015; Vibe, 1958), which are likely to be more common with the ensuing warming of the Arctic (Schmidt et al., 2019).

In this study, we have provided possible explanations for how the muskox not only persists, but appears to thrive today, despite a history of population declines due to environmental and anthropogenic factors. Studying a diverse range of wild species and demographic scenarios is imperative for unraveling the evolutionary processes associated with near-extinction population histories. Our results add to the growing body of literature illuminating how species with low genetic diversity escape the extinction vortex.

Methods

Ancient Siberian sample

Sampling

The ancient muskox sample was collected by one of us (S.V.) during field work on Wrangel Island. This sample was radiocarbon-dated at The Tandem Laboratory, Uppsala (Ua-21321; uncalibrated C14 date: 17655±215) and was calibrated to calendar age of 21,395 calBP using OxCal4.4 (Ramsey, 2009) with the IntCal20 calibration curve (Reimer et al., 2020) and median age estimate.

DNA extraction & Library preparation

Lab analyses were performed in the dedicated ancient DNA laboratory at the Swedish Museum of Natural History in Stockholm. Approximately 50mg of bone powder was collected from the sample using a Dremel drill. DNA was extracted from the bone powder following Yang et al.(Yang et al., 1998), with modifications as per Brace et al(Brace et al., 2012). Dual indexed double stranded Illumina DNA libraries were prepared from the DNA extract following Meyer and Kircher (Meyer & Kircher, 2010), with the addition of a USER-enzyme treatment prior to blunt end repair to remove DNA damage caused by deamination of cytosine to thymine (Pečnerová, Díez-Del-Molino, et al., 2017).

Sequencing

DNA libraries were sequenced on one lane of the NovaSeq6000 S4 platform in a 2x100bp setup at Science for Life Laboratory in Stockholm, Sweden in order to reach the target depth of high coverage (10X).

Mapping

Raw reads were demultiplexed using bcl2Fastq v1.8.3 (CASAVA software suite). Raw fastq reads were processed using the historical track of a development version of GenErode (Kutschera et al., 2022), where adapter trimming and merging was performed using SeqPrep (https://github.com/jstjohn/SeqPrep) with a small modification to the source code that allows for selecting the best quality scores of bases in the merged region, as per Palkopoulou et al. (2015). Reads were mapped separately to three reference genomes: 1) the new muskox genome assembly generated here; 2) the muskox genome assembly merged together with a previously published muskox mitochondrial genome available from GenBank under accession number NC020631 (Hassanin et al., 2009); and 3) a sheep (*Ovis aries*) genome assembly GCF_002742125.1 (*Oar_rambouillet_v1.0*, 2017a).

Modern samples

Samples

In this study, we performed whole-genome sequencing on a set of muskox samples that were previously used in a study based on reduced-representation sequencing (Hansen *et al.*, 2018). In addition, we sampled two new locations, in North Greenland (RY) and East Greenland (HD). The samples used in this study (Table S1; Figure S1) consisted primarily of skin,

muscle tissue, and blood. A large part of these samples was collected opportunistically, which influenced the quality.

DNA extraction

We extracted DNA using the QIAGEN DNeasy Blood & Tissue Kit (Valencia, CA, USA) following the manufacturer's instructions, with the exception of adding RNase A to get RNA-free genomic DNA. DNA quality was assessed on Qubit 2.0 Fluorometer, Nanodrop, and gel electrophoresis.

Sequencing

DNA libraries for most samples (except HD and RY) were prepared and sequenced by BGI China. Illumina libraries were prepared for whole genome sequencing in the 2x150bp paired-end setup and targeting either low (4X) or high (15X) coverage on the Illumina NovaSeq6000 S4 platform. In total, ~38 billion reads were generated for the 169 samples. For samples from the HD and RY locations, Illumina library preparation and sequencing were performed at the Science for Life Laboratory in Stockholm, Sweden. For these, we also used a 2x150bp paired-end sequencing, targeting high coverage and using 0.75 of an Illumina NovaSeq6000 S4 lane, which yielded ~3.8 billion reads.

Mapping

The sequencing data was mapped to the same three reference genomes as described above: 1) a muskox genome assembly (Li et al., 2023); 2) the muskox genome assembly merged together with a previously published muskox mitochondrial genome available from GenBank under accession number NC020631 (Hassanin et al., 2009); and 3) a sheep (*Ovis aries*) genome assembly GCF_002742125.1 (*Oar_rambouillet_v1.0*, 2017a).

For all three mapped datasets, we used a pipeline developed in Snakemake v5.6.0 (Mölder et al., 2021) and published in a modified version in (Pečnerová et al., 2021). The major modification compared to the originally published version of the pipeline is that here we use AdapterRemoval v2.3.0 (Schubert et al., 2016) for trimming and collapsing the sequencing reads (with default settings). The collapsed reads and the uncollapsed read pairs were then mapped separately using BWA v0.7.17 with the MEM algorithm (Li, 2013) and default settings. The alignments were processed (sort, fixmate, calmd, markdup), and collapsed and uncollapsed reads were merged per each sample using SAMtools v1.9 (Li et al., 2009). SAMtools were also used to index the alignments and generate statistics (flagstat, idxstats, stats). In a subsequent filtering step, we removed reads with mapping quality <MQ30, unmapped reads, duplicated reads, and secondary alignments. FastQC v0.10.1 (Andrews, 2010) and MultiQC v1.7 (Ewels et al., 2016) were used to generate and aggregate statistics before and after the mapping, as well as after filtering (Table S9).

For the merged nuclear-mitochondrial muskox reference, we extracted the reads that mapped to the mitogenome and generated two alignments, one where we applied a strict mapping quality filter of MQ30 and one without the mapping quality filter. The reads mapped to the nuclear part of the reference were not used in further analyses.

Reference Quality Filtering

For the muskox reference, we removed all scaffolds below 1MB in size in order to avoid the noise that the shorter scaffolds can introduce. This reduced the number of scaffolds from

7,071 to 134, but only reduced the size of the reference by ~2.5% to 2,552,915,699 bp. Unless otherwise noted, all subsequent reference quality filtering steps were performed for both the muskox and the sheep reference.

Removing sex scaffolds/chromosomes

Only autosomes were used for the subsequent analyses. Since the muskox reference does not contain information about sex scaffolds, we identified potential sex-linked scaffolds using a custom script to examine patterns of differential depth distribution, which was originally used in (Pečnerová et al., 2021), and later was published in an updated form as the SATC method (Nursyifa et al., 2022). After removing scaffolds with suspicious patterns of depth, we retained 79 presumably-autosomal scaffolds (Figure S24).

We used the published version of SATC (Nursyifa et al., 2022) to estimate the sex of our samples, and we also inferred sex using the sheep-mapped data since the sheep reference is chromosome-level and contains information on sex chromosomes (Table S11). The sheep reference is generated from a female sheep and contains only chromosome X. Thus, following the approach used in (Pečnerová, Díez-Del-Molino, et al., 2017) we compared the proportion of reads mapping to the chromosome X and an autosome of similar size (here, chromosome 3), normalized by the size of the chromosome (Table S11).

Repeat masking

For the sheep reference, a RepeatMasker file was available for download together with the genome file (*Oar_rambouillet_v1.0*, 2017b). For the muskox reference, we identified repetitive and low quality regions in the reference using RepeatModeler v2.0.1 (Flynn et al., 2020) and RepeatMasker v4.1.0 (A. F. A. Smit et al., 2019). The database rmblast v2.10.0 (A. Smit & Hubley, 2017) was used to build the database. RepeatMasker was run with the -gccalc option.

Mappability

We evaluated the mappability of each site in the reference using GEM (Derrien et al., 2012). The mappability was estimated with kmers of 150 bp and allowing for 2 mismatches and 2 differences (-m 0.0134 -e 0.0134 -l 150). Only sites with a mappability of 1 (i.e. uniquely mapping) were retained.

Global Sequencing depth

We also filtered out sites that had extreme depth across all samples. Using a custom Snakemake (Mölder et al., 2021) pipeline, and scripts in R v3.4.4 (R Core Team, 2018) and python (Van Rossum & Drake, 2009), we identified and excluded sites with less than a third or more than two times the median coverage at any genomic site. The depth was calculated separately for low-coverage and for high-coverage samples and then combined into a global depth, which was used to generate a bed file of sites to exclude.

Excessive heterozygosity filter

Some regions in the genome show excessive heterozygosity. To identify these, we inferred per-site inbreeding coefficients (F). We used ANGSD v0.929 (Korneliussen et al., 2014) to

15

generate a preliminary beagle file with genotype likelihoods for common polymorphic sites passing mapping and base quality filters and present in at least half of the samples (-gl 2 -doGlf 2 -doMajorMinor 1 -minMapQ 30 -minQ 30 -SNP_pval 1e-6 -doMaf 1 -minInd 54 -minMaf 0.05). The beagle file served as input for PCAngsd v0.99 (Meisner & Albrechtsen, 2018), which was used to calculate the per-site inbreeding coefficients (-inbreedSites) and to perform a Hardy-Weinberg Equilibrium (HWE) likelihood ratio test while accounting for population structure (Meisner & Albrechtsen, 2019). We used a custom R script to identify sites with excessive heterozygosity ($F < -0.95$ and p-value $< 10^{-6}$) and to remove these along with flanking regions of 50,000 bp around these sites. We also removed complete scaffolds if at least 20% of their total sequence was removed or if the average F for the whole scaffold was below -0.2.

Sample filtering

Error rates

We used the 'perfect-sample' approach (Orlando et al., 2013) to identify samples with relatively elevated error rates, which might be indicative of various problems with the samples (e.g. contamination or mis-identification). We used ANGSD (Korneliussen et al., 2014) to identify samples with a relative excess or deficit of derived alleles from the outgroup compared to the 'perfect sample'. This analysis was based on the sheep-mapped data and we used the sheep reference fasta file as the outgroup (-anc) and the HD-3 sample as the 'perfect sample' since it had been sequenced to the highest coverage. A consensus fasta sequence was generated for the HD-3 sample using the -doFasta 1 option in ANGSD. For the 'perfect-sample' analysis, we considered a randomly selected base (-doAncError 1) with a mapping and base qualities of at least 30 and only autosomes (-minMapQ 30 -minQ 30 -rf autosomes).

Deamination patterns

Since some of our samples showed elevated error rates, we used mapDamage v2.0.9 (Jónsson et al., 2013) to assess deamination patterns indicative of DNA degradation. We also used PMDtools to compare the deamination-derived damage patterns in CpG and non-CpG sites (Skoglund et al., 2014).

Identification of related or duplicated samples

We used ngsRelate v2 (Hanghøj et al., 2019) to calculate the KING/R0 and R1 statistics (Waples et al., 2019) to identify pairs of potentially duplicated or closely related samples. Samples were grouped into regions (listed in Table S1) and genotype likelihoods and population allele frequencies were generated for each region in ANGSD (Korneliussen et al., 2014) using the same settings as described in the section '*Reference Quality Filtering: Excessive heterozygosity filter*', but without the minimum number of individuals filter (-minInd). One pair of samples was identified as duplicates based on the results (BI-32 and BI-38) and one sample of the pair was then removed from further analyses (BI-38).

QC summary

Out of 178 modern muskox genomes sequenced, only 107 passed our sample quality filters. A surprisingly high proportion of samples yielded low endogenous DNA levels and high error rates (Figure S25; Table S9); however, deamination patterns do not seem to indicate that these samples are ancient (Figure S26). This concerned both samples sequenced at BGI China and

16

SciLifeLab Stockholm, ruling out issues in sequencing technology. We hypothesize that this pattern is most likely caused by these samples having been collected opportunistically, sometimes as tissue flakes from older carcasses. Due to the nature of the Arctic environment and slow decomposition, these muskox remains might have lain on the surface longer than immediately obvious (but not in an ancient DNA context), while being exposed to the weather conditions, UV radiation, and contamination, which resulted in poor DNA preservation. Other reasons for samples being excluded from further analyses included species misidentification (TH-17 and TH-24) and sample duplication (BI-32 and BI-38).

The ancient Siberian sample showed slightly elevated error rates compared to the modern-day samples passing our filters (Figure S25), which likely result from ancient DNA damage at the CpG sites (Figure S27), where the USER treatment removing damage is not effective.

Reliability of the ancient-modern sample comparisons

To ensure that the downstream analyses of the ancient genome are comparable to the estimates from modern samples, we undertook several measures. Firstly, we built the sequencing library using a protocol that incorporates USER treatment, which removes DNA damage (Meyer & Kircher, 2010; Pečnerová, Díez-Del-Molino, et al., 2017). Secondly, we used mapDamage v2.0.9 (Jónsson et al., 2013) to confirm that the USER treatment was overall effective and the ancient genome does not deviate from the damage patterns observed in our modern samples (Figure S26). Third, we estimated the effect of CpG sites, in which the USER treatment is not effective and DNA damage might have caused slightly elevated error rates (Figure S27). By comparing heterozygosity with and without applying a CpG filter, we verified that the diversity of the ancient sample is not driven by DNA damage in CpG sites as the effect of the filter did not differ markedly compared to the modern samples (Table S4). In addition, we estimated heterozygosity from SFS (see below section 'Heterozygosity and Inbreeding') both including and excluding transitions, which are commonly affected by ancient DNA damage, and we did not observe a marked difference in the effect of this filter between the ancient and the modern samples (Figure S18). In the analyses of genetic load focused on derived alleles, which are most sensitive to errors, we filtered out CpG sites. Yet, we still see a slight excess of derived alleles in the ancient Siberian genome, and we take this into consideration when interpreting ou results with care.

Datasets

To perform a range of different analyses, we generated six datasets (Table S12): 1) muskoxmap: modern samples mapped to the muskox reference; 2) muskoxmap_wSib: modern samples and the ancient Siberian sample mapped to the muskox reference; 3) muskoxmap_wSib_wSheep: modern samples, the ancient Siberian sample, and a sheep genome (a male Texel sheep Illumina paired-end data available from the European Nucleotide Archive under accession PRJEB6251) as an outgroup, all mapped to the muskox reference; 4) sheepmap: modern samples mapped to the sheep reference; 5) sheepmap_wSib: modern samples and the ancient Siberian sample mapped to the sheep reference; 6) sheepmap_wSib_wSheep: modern samples, the ancient Siberian sample and sheep as an outgroup, all mapped to the sheep reference.

Genotype likelihoods

Since a part of our samples was sequenced to low depth, we based many of the population genomic analyses on genotype likelihoods rather than called genotypes. We estimated genotype likelihoods and exported them in beagle format using ANGSD (Korneliussen et al.,

17

2014) and the GATK model (-gl 2). We estimated the allele frequencies (-doMaf 1) and the major and minor allele from the data (-doMajorMinor 1). We also filtered for base and mapping qualities of at least 30 (-minMapQ 30 -minQ 30), using only the scaffolds and sites that passed all the filters in the 'Reference Quality Filtering' sections. We took into consideration common mutations validated by the likelihood ratio test with p-value = 10^{-6} and having sequencing data present in at least half of the individuals (-minMaf 0.05 -SNP_pval 1e-6 -minInd 54).

Genotype calls

We called genotypes for high quality samples, i.e. samples passing all QC filters and having a depth of coverage on sites of interest (passing all filters in 'Reference Quality Filtering') of at least 9.5X (Table S9). Genotype calling was done using a custom Snakemake v5.6.0 (Mölder et al., 2021) pipeline. We called the genotypes per sample using bcftools v0.1.19 (Li, 2011) and the multiallelic caller method (-m), with disabled base alignment qualities (BAQ; -B), filtering for base qualities of at least 30, only taking into consideration the sites passing the filters in 'Reference Quality Filtering'. To reduce spurious calls, we excluded sites with a depth of coverage below 10 and heterozygous calls with less than three reads supporting each allele by applying the setGT plugin. For the analyses of genetic load, in order to increase the number of sites analysed and based on the fact that the vast majority of genotypes are homozygous, we called variants with more lenient filters, excluding a depth of coverage below five and heterozygous calls with less than two reads supporting each allele, and we verified that this does not introduce bias as heterozygosity remains stable. For the genetic load variant calling, we included the CpG filter since the analysis is particularly sensitive to derived alleles.

Population structure

PCA analyses

We investigated population structure in PCAngsd (Meisner & Albrechtsen, 2019) using the beagle file with genotype likelihoods from ANGSD (Korneliussen et al., 2014) as input and four eigenvectors to model the structure. The results were plotted using the package 'ggplot2' (Wickham, 2021) in RStudio v1.2.5001 (Rstudio Team, 2019). We simultaneously inferred a neighbor-joining tree (-tree) in PCAngsd (Meisner & Albrechtsen, 2018) and visualised the results in FigTree v.1.4.4 (Rambaut, 2014).

NGSadmix and evalAdmix

We used NGSadmix (Skotte et al., 2013) to evaluate admixture proportions based on genotype likelihoods. We ran NGSadmix for K=5 to K=13. To evaluate convergence, we ran a number of independent runs either until reaching three top maximum likelihood results within 2 log-likelihood units of each other, or until 100 runs ended without convergence. Only K=5-8 reached convergence. We evaluated the resulting model fit with evalAdmix v0.95 (Garcia-Erill & Albrechtsen, 2020), which shows positive pairwise correlation of residuals between individuals from similar ancestry if the model has a poor fit to the data.

Genetic distance tree

We evaluated genetic clustering based on genetic distances by building a neighbor-joining (NJ) tree (Saitou & Nei, 1987) based on an identity-by-state (IBS) matrix. We used the -

doIBS 1 option in ANGSD (Korneliussen et al., 2014) to generate the IBS matrix of pairwise genetic distances, applying the same settings as listed in the 'Genotype likelihoods' section. For this analysis, we used the sheep-mapped dataset, including the ancient Siberian sample (SIB) and the sheep. The results were plotted in RStudio v1.2.5001 (Rstudio Team, 2019) using R packages 'dplyr', 'ape' (Paradis & Schliep, 2019), and 'phangorn' (K. Schliep et al., 2017; K. P. Schliep, 2011). The tree was visualized in FigTree v.1.4.4 (Rambaut, 2014).

EEMS

We calculated the IBS matrix in the same way as described in the '*Genetic distance tree*' section, but in this case, we used the muskox-mapped dataset without the Siberian or sheep samples. We used the IBS matrix to calculate relative migration rates using the Estimation of Effective Migration Surfaces (EEMS) (Petkova et al., 2016). Besides the IBS matrix, the input also consisted of the geographic coordinates of the samples (Table S1) and an outline of the region manually drawn using the tool available here: http://www.birdtheme.org/useful/v3tool.html. In EEMS, we ran three chains of the runeems_snps program at default settings and with 10,000,000 steps, burn-in of 2 million steps, 400 demes and 1,444,546 sites from the IBS matrix.

We used the make_eems_plots function implemented in the R package 'reemsplots2' available from https://github.com/dipetkov/reemsplots2 along with R packages 'dplyr', 'ggplot2' (Wickham, 2021), and 'coda' (Plummer et al., 2006) to visualize the results and evaluate convergence of the three runs. The convergence was estimated using the Gelman-Rubin diagnostic test (Gelman & Rubin, 1992) and the resulting scale reduction factor of 1.08 indicated convergence. Results were visualized as log10-transformed relative migration rates with posterior probabilities >0.90.

D-statistics based on genotype calls

We used admixtools2 (available from https://uqrmaie1.github.io/admixtools/index.html; (Patterson et al., 2012)) to estimate *D*-statistics using genotype calls from the data mapped to the sheep, for all triplets pairing modern samples as P1 and P2, and the ancient Siberian sample as P3. We used the reference allele in the sheep genome as the outgroup P4. We used all non-missing SNPs for each triplet, and subsequently removed triplets where less than 1 million SNPs were left after removing missing positions. We used 5 MB blocks to estimate standard errors using the built-in block jackknife procedure (Busing et al., 1999; Patterson et al., 2012). For plotting, we excluded triplets involving individuals from GrES (HD and JA), for which the long runs of homozygosity made the 5 Mb block size inadequate and showed biased results.

F_{ST}

We evaluated the extent of population differentiation with the fixation index F_{ST} measured by two approaches based on 2d site frequency spectra (SFS): per-population approach based on genotype likelihoods and individual pairwise approach based on called genotypes.

Site frequency spectrum

We estimated SFS using realSFS v0.931 (Nielsen et al., 2012) implemented in ANGSD (Korneliussen et al., 2014). We first estimated one-dimensional (1d) SFSs per population by generating saf files in ANGSD using the -doSAF 1 option, the GATK model (-gl 2), filtering for mapping and base qualities (-minQ 30 -minMapQ 30) and only using the sites passing the

filters in 'Reference Quality Filtering' (Figure S28). The 1d SFS SAF files were used in realSFS for two-dimensional (2d) SFS calculation of all pairs of populations. From the 2dSFS we directly calculated genome-wide F_{ST} using the Reich estimator (Reich et al., 2009).

Genotype-call-based SFS

We also estimated F_{ST} by generating 1dSFS from per-individual genotype calls and subsequently generating 2dSFS between all pairs of individuals using custom scripts. As above, the global F_{ST} was calculated using the Reich estimator (Reich et al., 2009) and averaged across pairs of populations.

Heterozygosity & Inbreeding

To obtain genome-wide heterozygosity estimates, we used three different approaches: per-samples 1d SFS from genotype likelihood, direct counts from genotype calls, and ROHan from genotype likelihoods (Renaud et al., 2019).

SFS-based

We calculated the SFS following the same approach as described in '*F_{ST}: Site frequency spectrum*', but also filtering out sites with depth of coverage below three (-setMinDepth 3). We used realSFS (Nielsen et al., 2012) to fold the SFS (-fold 1) in the absence of ancestral-state information, and to generate the estimate of the proportion of heterozygous sites.

Genotype-call-based

We used a custom Snakemake v5.6.0 (Mölder et al., 2021) pipeline incorporating bcftools (Li, 2011) to output summary statistics, remove indels, and calculate the proportion of heterozygous sites in the vcf files generated in section *Genotype calls*.

ROHan

ROHan v1.0 (Renaud et al., 2019) was applied to perform a joint estimation of global heterozygosity rates and runs of homozygosity (ROH). The analysis was performed with default settings on bam files, which were filtered to remove QC-failing reads and duplicates (-F 3844) but were not filtered for mapping and base quality, since that information is used in the calculation of the genotype likelihoods. We only used the sites passing all filters in the "*Reference Quality Filtering*". The heterozygosity estimates from ROHan were overestimated for the least diverse individuals because there is a hard cap on the minimum heterozygosity of 0.0008. Below this, ROHan (Renaud et al., 2019) cannot distinguish between heterozygosity within and outside ROH.

PLINK

We also estimated ROH based on the genotype calls in PLINK v1.9 (Chang et al., 2015; Purcell & Chang, 2015). For estimating the ROH inbreeding coefficient, we took into consideration ROH at least 1 MB in size (--homozyg-kb 1000). For more detailed insights into the size distribution of ROH, we also reported ROH in size categories of 0.5-1 MB, 1-2 MB, 2-5 MB, 5-10 MB and at least 10 MB (Figure S19). Due to the stringent quality filters (minimum depth of 10 and a support of at least three alleles for a heterozygous call; see 'Genotype calls'), we used a high limit for missing sites (--homozyg-window-missing 40).

Demographic history

PSMC

We estimated the trajectory of effective population sizes through time using the Pairwise Sequentially Markovian Coalescent (PSMC) model (Li & Durbin, 2011). Following the recommended procedure, we used bcftools v1.9 (Li, 2011) with the -c option to call genotypes and applied the same filtering procedure as described in 'Heterozygosity: Genotype calls'. We applied PSMC with default settings, and for plotting we scaled the result with a mutation rate of $1x10^{-8}$ per site per year and generation time of 8 years (Hansen et al., 2018). We removed the five most recent time points in all samples to account for the inability of PSMC to accurately estimate population size in recent times (equating to ~500-1000 years in the modern samples).

PopSizeABC

PopSizeABC was used to estimate changes in population sizes using multiple samples from the same population. To give reliable results PopSizeABC requires sufficiently large sample sizes (i.e. > 9 individuals) per population in order to give reliable population size estimates. This allowed us to estimate population size changes in four populations; CaME (14 individuals), CalS (10 individuals), CaMW (10 individuals) and ZA (11 individuals).

PopSizeABC estimated LD curves and SFS for tested populations from a vcf file containing the populations under study based on data mapped to the sheep reference genome. The same recombination rate and mutation rate used in PSMC were used in POPSIZEABC. PopSizeABC also requires multiple simulations of demographic scenarios to compare a posterior distribution of simulation derived parameters to those observed in the real data. For each population, 30,000 simulations were performed for 100 2-Mb regions per simulation as per the suggested settings in the publication for the software. For both the summated and target populations a minimum MAF threshold of 0.1 SFS and 0.2 for calculation of the LD curves, again in accordance with the suggested parameters in the PopSizeABC publication.

Mitogenome tree and dating

Since there is evidence of mitochondrial insertions in the nucleus (NuMts) in the muskox (Kolokotronis et al., 2007), we performed a competitive mapping of our sequencing data to a merged reference containing both, the muskox nuclear genome assembly and a published mitochondrial genome available from GenBank (accession number: NC020631) (Hassanin et al., 2009). This competitive mapping ensures that the nuclear insertions of mitochondrial sequences will map preferably to their location in the nuclear genomes, and that the reads mapping to the mitogenome do originate from mitochondria or that the two are indistinguishable. The reads mapping to the mitochondrial part of the merged reference genome were then extracted using SAMtools v1.9 (Li et al., 2009) and uploaded to Geneious Prime® v2019.1.1 (Kearse et al., 2012), where we generated consensus sequences using strict 50% call. We called only positions with coverage of at least 10 reads for the alignment of only modern mitogenomes and if at least 5 reads for the alignment with previously published sequences of the control region (ct-region) from ancient samples. For both alignments, we aligned the consensus sequences in MAFFT v7.307 (Katoh & Standley, 2013) and we generated a median-joining network in POPart v1.7 (Bandelt et al., 1999; Leigh et al., 2015). Sheep mitochondrial genome (Genbank ID: NC_001941.1) was used as an outgroup.

To generate a phylogenetic tree, we also chose a substitution model in ModelTest-NG v0.1.7 (Darriba et al., 2020), specifying the -mrbayes selection of substitution schemes to fit the selection in BEAST. We generated a mitogenome tree in BEAST v2.6.3 (Bouckaert et al.,

2019) using a strict clock with a mutation rate of 8.7×10^{-7} substitutions per site per generation previously estimated for mitochondrial DNA in muskox (Campos et al., 2010), coalescent constant population tree model, and GTR-G4 substitution model.

In addition, for the alignment including ct-region ancient sequences, we used tip-dating based on ages of the ancient samples (Campos et al., 2010), which we calibrated to calendar age using OxCal4.4 (Ramsey, 2009) with the IntCal20 calibration curve (Reimer et al., 2020) and median of the ages. Only sequences with finite radiocarbon dates were included in the phylogeny. The resulting alignment consisted of 194 samples and 875 sites. The alignment including full mitogenomes of the samples generated in this study included 109 individuals and 16746 sites.

We ran the analysis for 10 million generations, with a pre-burn-in of 1000 steps, logging trees every 1000 steps. We used Tracer v1.7.1 (Rambaut et al., 2018) to assess the convergence of the run and we used TreeAnnotator v2.6.3 to generate a maximum clade credibility tree with a burn-in of 30%, considering only posterior probabilities above 0.7 and choosing median heights for node heights. The tree was visualized in FigTree v.1.4.4 (Rambaut, 2014).

Nuclear dating

To generate a dated nuclear phylogeny using iqtree v2.2.0 (Minh et al., 2020) a subset of the dataset was used. This encompassed the highest coverage genome per geographic region (SIB: EL012; CaME: BL-11; CaMW: KU-23; CaIS: AI-1; CaIN: SF-1; GrN: RY-3; GrEN: MO34; GrES: HD-3) and the sheep as an outgroup. Random allele sampling was performed using the ANGSD -dohaplocall 1 option, with the following settings: --uniqueOnly 1, -remove_bads 1, -minMapQ 30 -minQ 30, -doCounts 1, -minMinor 1. Only sites included in the whitelist bed file were analysed using the -sites option. Haploid called files were subsampled for every 100th line using awk. Called files were then converted to FASTA format using a custom python script. A neighbour-joining phylogenetic tree was constructed from the fasta files using MEGAX (Stecher et al., 2020). The divergence dating option in Iqtree v2.2.0 was used to build a dated phylogeny, with the NJ tree specified as the input tree (-te option) (To et al., 2016). The age of the Siberian sample (21,395 years old) and earliest fossil evidence of muskox in Greenland at 4,500 years ago (Bennike & Andreasen, 2005; Campos et al., 2010) were used as calibration points. The tree was visualised in Figtree v4.3.3 (Figure S29).

Twisst

Since the nuclear and mitochondrial tree yielded incongruent topologies, we also ran Twisst v0.2 (Martin & Van Belleghem, 2017), which explores how topologies vary along the genome. We used ANGSD (Korneliussen et al., 2014) and the -doIBS command following the same approach as above, but this time for each 100 kb window. Then we used Twisst for weighting the topologies and visualizing the alternative topologies along the chromosomes. However, the analyses yielded unreasonable results, which can be likely attributed to the lack of power at low-variation conditions (Figure S30).

TreeMix

For each population, we called the maximum-likelihood sample frequency based on the SAF-files to make the TreeMix input. Only sites found in SAF files for all populations were considered, leaving approximately 1.22 million sites. Using this input, we ran TreeMix using

a block size of 2025 and specifying the sheep as an outgroup. For each number of allowed migrations from zero through three, we ran 25 independently seeded replicates and chose the TreeMix result with the highest log-likelihood.

qpGraph

We used qpGraph (Patterson et al., 2012) to explore admixture graph topologies of the main muskox lineages. We used genotype calls from the data mapped to the sheep reference. To simplify the search space and avoid biases due to the low amount of variation, we excluded the GrEN and GrE populations from the analysis. We used a pseudo haploid sheep as an outgroup population, generated by taking the allele in the sheep reference genome. We applied the automatic graph optimizing findGraphs function from ADMIXTOOLS2 (Maier et al., 2022), running 50 optimization runs allowing for up to 2 migration events, without any topological restrictions. We selected as the best fitting graph, the one that did not have any significantly deviating residuals between the model and the data and that had the best score.

Genetic load

We used two complementary approaches to estimate genetic load, from the functional annotation or conservation scores as proxy for fitness.

GERP conservation scores

GERP scores were calculated using the GenErode pipeline (Kutschera et al., 2022). A set of 50 mammalian genomes retrieved from NCBI were included as outgroups (Table S13). A newick tree was produced using TimeTree (http://timetree.org/), with all outgroup species and the target species. Briefly, the outgroup genomes were mapped to the muskox reference genome using BWA mem v0.7.17 (Li, 2013). GERP scores were computed for each position in the reference genome using GERP++ v2.1 (Davydov et al., 2010). The GERP scores were then converted to genomic coordinates and rescaled to time in billions of years using the dated phylogeny produced with TimeTree. The ancestral state for each position in the reference genome was determined and then merged with the corresponding GERP score. Genotype calls for the muskox-mapped data with more lenient filters (see section *Genotype calls*) were used as input, and subsequently filtered for biallelic sites, sites within 5bp of indels. Derived alleles were defined as differing from the ancestral state shared by all taxa in the multispecies alignment. We estimated the relative load at a set of 1,746,415 sites with less than 10% missingness (Figure 4C), as well at 277,370 sites represented in all individuals, i.e. with 0% missingness (Figure S20).

Functional annotation

SnpEff (Cingolani et al., 2012) was used to annotate the VCF by different impact categories (high, moderate, low, and modifier) using the GenErode pipeline (Kutschera et al., 2022). Genotype calls for sheep-mapped data were used with the same lenient filters as above, and filtered for biallelic sites and 0% missing data. The load was estimated on 2,309,442 sites analyzed.

Calculating genetic load

We then used four different measures of calculating genetic load using the annotation from GERP or SnpEffs. They are all based on data where across all individuals there are M variable sites where at least one individual has a derived allele. This also includes sites where every individual is homozygous for the derived allele.

23

First, for individual i at site j we used the number of derived alleles $d_{ij} \in \{0,1,2\}$ and the GERP conservation score to calculate the relative load

$$\textbf{relative load: } loadG_i = \frac{\sum_{j=1}^{M} GERP_j \, d_{ij}}{\sum_{j=1}^{M} d_{ij}} = \frac{sum \ of \ GERP \ scores \ per \ derived \ allele}{Number \ of \ derived \ alleles} \, ,$$

which is the average GERP conservation scores of the derived alleles that fall within a minimum and maximum threshold of GERP scores (0 and 1000, respectively, as indicative of an evolutionary constraint).

Second, based on functional annotation we categorized each variable site into putative impact defined in SnpEff: high impact (stop-gain and frameshift variants), moderate impact (missense variants and in-frame deletions), low impact (synonymous variants), and modifier impact (non-coding variants).

For all of the methods below, for each individual we took a subset of the genotypes where this individual has at least one derived allele (i.e. differing from the ancestral state in the sheep outgroup). Specifically, each site j is given a functional category s_j. For a certain category c with M_{ic} sites out of M_i sites that are variable for individual i. Here $I_{1,2}$ is an indicator functions that takes the value 1 if you have at least one derived allele i.e. $d_{ij}>0$ and zero otherwise. Similarly, I_c is an indicator function that takes the value 1 if the category s_j of site j is c and zero otherwise. Note that for a single individual a variable site is defined as having at least one derived allele.

First, we calculated the number of derived alleles in each of the different categories per 100,000 derived alleles (Figure 7, Figure S21, Figure S22). In other words, we count ((2*HO derived alleles + 1*HE derived alleles of the impact category)/total derived alleles)*100,000 or

$$\textbf{total load: } \frac{LoadT_{ic}}{100000} = \frac{\sum_{j=1}^{M} d_{ij} I_c(s_j)}{\sum_{j=1}^{M} d_{ij}} = \frac{\#derived \ alleles \ at \ category \ type \ c \ sites}{total \ number \ of \ derived \ alleles} \, .$$

Second, we took the same subset of sites, but rather than calculating individual derived alleles, we calculated the fraction of each of the different categories among these sites as the potential load:

$$\textbf{potential load: } LoadP_{ic} = \frac{\sum_{j=1}^{M} I_{1,2}(d_{ij}) I_c(s_j)}{\sum_{j=1}^{M} I_{1,2}(d_{ij})} = \frac{M_{ic}}{M_i} = \frac{\#variable \ sites \ of \ category \ type \ c}{total \ number \ of \ variable \ sites} \, ,$$

which is simply the fraction of genotypes with one or two derived alleles with a certain functional annotation.

Third, we calculated the recessive realized load using the same functional annotation as for potential load. Here, or a certain category c with M_c sites we have

recessive realized load: $LoadR_{ic} = \dfrac{\sum\limits_{j=1}^{M} I_2(d_{ij}) I_c(s_j)}{2\sum\limits_{j=1}^{M} I_{1,2}(d_{ij}) I_c(s_j)} = \dfrac{\#derived\ homozygous\ sites\ of\ type\ c}{\#alleles\ at\ variable\ sites\ of\ type\ c}$

This recessive realized load is the fraction of variable sites that are homozygous within a certain category.

Limitations of low-variation data

In several of the analyses, we ran into the limitations associated with analyzing extremely low-variation data. Most markedly, this concerns analyses of PSMC, ROHan, *D*-statistics, and qpGraph, where the most homozygous populations from Greenland failed to yield robust results due to the low number of informative sites available. In PSMC, this was observed as outlier trajectories in the Greenlandic population, driven by the low number of coalescence events in deeper time (Figure S15). In ROHan, this was reflected in the Greenlandic populations hitting the cap of minimum heterozygosity level of 0.8×10^{-4}, even though some individuals had lower heterozygosity estimated by other methods (Table S4). In *D*-statistics and qpGraph, we removed the two most homozygous populations from East Greenland because the long runs of homozygosity made the 5 Mb block size inadequate and showed biased results. This illustrates some scenarios where the current population genetic tools, mostly developed for better-quality human datasets, fall short.

Acknowledgements

References

Abascal, F., Corvelo, A., Cruz, F., Villanueva-Cañas, J. L., Vlasova, A., Marcet-Houben, M., Martínez-Cruz, B., Cheng, J. Y., Prieto, P., Quesada, V., Quilez, J., Li, G., García, F., Rubio-Camarillo, M., Frias, L., Ribeca, P., Capella-Gutiérrez, S., Rodríguez, J. M., Câmara, F., … Godoy, J. A. (2016). Extreme genomic erosion after recurrent demographic bottlenecks in the highly endangered Iberian lynx. *Genome Biology, 17*(1), 251.

Andrews, S. (2010). *FastQC: a quality control tool for high throughput sequence data* (Version 0.10.1) [Computer software]. https://www.bioinformatics.babraham.ac.uk/projects/fastqc/

Atwood, T. B., Valentine, S. A., Hammill, E., McCauley, D. J., Madin, E. M. P., Beard, K. H., & Pearse, W. D. (2020). Herbivores at the highest risk of extinction among mammals, birds, and reptiles. *Science Advances, 6*(32), eabb8458.

Bandelt, H. J., Forster, P., & Röhl, A. (1999). Median-joining networks for inferring intraspecific phylogenies. *Molecular Biology and Evolution, 16*(1), 37–48.

Barr, W. (1991). The commercial trade in muskox hides in the Northwest Territpries 1860-1916. *Rangifer, 11*(2), 81–82.

Bennike, O., & Andreasen, C. (2005). Radiocarbon dating of musk-ox (Ovibos moschatus) remains from northeast Greenland. *The Polar Record, 41*(219), 305–310.

Bertorelle, G., Raffini, F., Bosse, M., Bortoluzzi, C., Iannucci, A., Trucchi, E., Morales, H. E., & van Oosterhout, C. (2022). Genetic load: genomic estimates and applications in non-model animals. *Nature Reviews. Genetics, 23*(8), 492–503.

Boitard, S., Rodríguez, W., Jay, F., Mona, S., Austerlitz, F. (2016). Inferring population size history from large samples of genome-wide molecular data - an approximate Bayesian computation approach. *PLOS Genetics, 12*(3), e1005877.

Bouckaert, R., Vaughan, T. G., Barido-Sottani, J., Duchêne, S., Fourment, M., Gavryushkina, A., Heled, J., Jones, G., Kühnert, D., De Maio, N., Matschiner, M., Mendes, F. K., Müller, N. F., Ogilvie, H. A., du Plessis, L., Popinga, A., Rambaut, A., Rasmussen, D., Siveroni, I., … Drummond, A. J. (2019). BEAST 2.5: An advanced software platform for Bayesian evolutionary analysis. *PLoS Computational Biology*, *15*(4), e1006650.

Brace, S., Palkopoulou, E., Dalén, L., Lister, A. M., Miller, R., Otte, M., Germonpré, M., Blockley, S. P. E., Stewart, J. R., & Barnes, I. (2012). Serial population extinctions in a small mammal indicate Late Pleistocene ecosystem instability. *Proceedings of the National Academy of Sciences of the United States of America*, *109*(50), 20532–20536.

Buffalo, V. (2021). Quantifying the relationship between genetic diversity and population size suggests natural selection cannot explain Lewontin's Paradox. *eLife*, *10*. https://doi.org/10.7554/eLife.67509

Busing, F. M. T. A., Meijer, E., & Leeden, R. V. D. (1999). Delete-m Jackknife for Unequal m. *Statistics and Computing*, *9*(1), 3–8.

Campos, P. F., Willerslev, E., Sher, A., Orlando, L., Axelsson, E., Tikhonov, A., Aaris-Sørensen, K., Greenwood, A. D., Kahlke, R.-D., Kosintsev, P., Krakhmalnaya, T., Kuznetsova, T., Lemey, P., MacPhee, R., Norris, C. A., Shepherd, K., Suchard, M. A., Zazula, G. D., Shapiro, B., & Gilbert, M. T. P. (2010). Ancient DNA analyses exclude humans as the driving force behind late Pleistocene musk ox (Ovibos moschatus) population dynamics. *Proceedings of the National Academy of Sciences of the United States of America*, *107*(12), 5675–5680.

Canteri, E., Brown, S. C., Schmidt, N. M., Heller, R., Nogués-Bravo, D., & Fordham, D. A. (2022). Spatiotemporal influences of climate and humans on muskox range dynamics over multiple millennia. *Global Change Biology*, *28*(22), 6602–6617.

Caughley, G. (1994). Directions in Conservation Biology. *The Journal of Animal Ecology*, *63*(2), 215–244.

Chang, C. C., Chow, C. C., Tellier, L. C., Vattikuti, S., Purcell, S. M., & Lee, J. J. (2015). Second-generation PLINK: rising to the challenge of larger and richer datasets. In *GigaScience* (Vol. 4, Issue 1). https://doi.org/10.1186/s13742-015-0047-8

Cho, Y. S., Hu, L., Hou, H., Lee, H., Xu, J., Kwon, S., Oh, S., Kim, H.-M., Jho, S., Kim, S., Shin, Y.-A., Kim, B. C., Kim, H., Kim, C.-U., Luo, S.-J., Johnson, W. E., Koepfli, K.-P., Schmidt-Küntzel, A., Turner, J. A., … Bhak, J. (2013). The tiger genome and comparative analysis with lion and snow leopard genomes. *Nature Communications*, *4*, 2433.

Cingolani, P., Platts, A., Wang, L. L., Coon, M., Nguyen, T., Wang, L., Land, S. J., Lu, X., & Ruden, D. M. (2012). A program for annotating and predicting the effects of single nucleotide polymorphisms, SnpEff: SNPs in the genome of Drosophila melanogaster strain w1118; iso-2; iso-3. *Fly*, *6*(2), 80–92.

Colella, J. P., Lan, T., Schuster, S. C., Talbot, S. L., Cook, J. A., & Lindqvist, C. (2018). Whole-genome analysis of Mustela erminea finds that pulsed hybridization impacts evolution at high latitudes. *Communications Biology*, *1*, 51.

Cuyler, C., Rowell, J., Adamczewski, J., Anderson, M., Blake, J., Bretten, T., Brodeur, V., Campbell, M., Checkley, S. L., Cluff, H. D., Côté, S. D., Davison, T., Dumond, M., Ford, B., Gruzdev, A., Gunn, A., Jones, P., Kutz, S., Leclerc, L.-M., … Ytrehus, B. (2020). Muskox status, recent variation, and uncertain future. *Ambio*, *49*(3), 805–819.

Dalén, L., Fuglei, E., Hersteinsson, P., Kapel, C. M. O., Roth, J. D., Samelius, G., Tannerfeldt, M., & Angerbjörn, A. (2005). Population history and genetic structure of a circumpolar species: the arctic fox. *Biological Journal of the Linnean Society. Linnean*

Society of London, 84(1), 79–89.

Darriba, D., Posada, D., Kozlov, A. M., Stamatakis, A., Morel, B., & Flouri, T. (2020). ModelTest-NG: A New and Scalable Tool for the Selection of DNA and Protein Evolutionary Models. *Molecular Biology and Evolution*, *37*(1), 291–294.

Davydov, E. V., Goode, D. L., Sirota, M., Cooper, G. M., Sidow, A., & Batzoglou, S. (2010). Identifying a High Fraction of the Human Genome to be under Selective Constraint Using GERP. In *PLoS Computational Biology* (Vol. 6, Issue 12, p. e1001025). https://doi.org/10.1371/journal.pcbi.1001025

Derrien, T., Estellé, J., Marco Sola, S., Knowles, D. G., Raineri, E., Guigó, R., & Ribeca, P. (2012). Fast computation and applications of genome mappability. *PloS One*, *7*(1), e30377.

Desforges, J.-P., Marques, G. M., Beumer, L. T., Chimienti, M., Hansen, L. H., Pedersen, S. H., Schmidt, N. M., & van Beest, F. M. (2021). Environment and physiology shape Arctic ungulate population dynamics. *Global Change Biology*, *27*(9), 1755–1771.

Díez-del-Molino, D., Sánchez-Barreiro, F., Barnes, I., Gilbert, M. T. P., & Dalén, L. (2018). Quantifying Temporal Genomic Erosion in Endangered Species. *Trends in Ecology & Evolution*, *33*(3), 176–185.

Durand, E. Y., Patterson, N., Reich, D., & Slatkin, M. (2011). Testing for ancient admixture between closely related populations. *Molecular Biology and Evolution*, *28*(8), 2239–2252.

Dussex, N., van der Valk, T., Morales, H. E., Wheat, C. W., Díez-del-Molino, D., von Seth, J., Foster, Y., Kutschera, V. E., Guschanski, K., Rhie, A., Phillippy, A. M., Korlach, J., Howe, K., Chow, W., Pelan, S., Mendes Damas, J. D., Lewin, H. A., Hastie, A. R., Formenti, G., … Dalén, L. (2021). Population genomics of the critically endangered kākāpō. *Cell Genomics*, *1*(1), 100002.

Ewels, P., Magnusson, M., Lundin, S., & Käller, M. (2016). MultiQC: summarize analysis results for multiple tools and samples in a single report. *Bioinformatics* , *32*(19), 3047–3048.

Falk, J. M., Schmidt, N. M., Christensen, T. R., & Ström, L. (2015). Large herbivore grazing affects the vegetation structure and greenhouse gas balance in a high arctic mire. *Environmental Research Letters: ERL [Web Site]*, *10*(4), 045001.

Fedorov, V. B., & Stenseth, N. C. (2002). Multiple glacial refugia in the North American Arctic: inference from phylogeography of the collared lemming (*Dicrostonyx groenlandicus*). In *Proceedings of the Royal Society of London. Series B: Biological Sciences* (Vol. 269, Issue 1505, pp. 2071–2077). https://doi.org/10.1098/rspb.2002.2126

Flynn, J. M., Hubley, R., Goubert, C., Rosen, J., Clark, A. G., Feschotte, C., & Smit, A. F. (2020). RepeatModeler2 for automated genomic discovery of transposable element families. *Proceedings of the National Academy of Sciences of the United States of America*, *117*(17), 9451–9457.

Foote, A. D., Alexander, A., Ballance, L. T., Constantine, R., Galletti Vernazzani Muñoz, B., Guinet, C., Robertson, K. M., Sinding, M.-H. S., Sironi, M., Tixier, P., Totterdell, J., Towers, J. R., Wellard, R., Pitman, R. L., & Morin, P. A. (2023). "Type D" killer whale genomes reveal long-term small population size and low genetic diversity. *The Journal of Heredity, 114*(2), 94–109.

Frankham, R. (1996). Relationship of genetic variation to population size in wildlife. *Conservation Biology: The Journal of the Society for Conservation Biology*, *10*(6), 1500–1508.

Franklin, I. R. (1980). *Evolutionary change in small populations*. https://publications.csiro.au/rpr/pub?list=BRO&pid=procite:46c4045a-9333-43d5-973b-6f55ad9a9cc8

Garcia-Erill, G., & Albrechtsen, A. (2020). Evaluation of model fit of inferred admixture proportions. *Molecular Ecology Resources*, *20*(4), 936–949.

Gelman, A., & Rubin, D. B. (1992). Inference from Iterative Simulation Using Multiple Sequences. *Schweizerische Monatsschrift Fur Zahnheilkunde = Revue Mensuelle Suisse D'odonto-Stomatologie / SSO*, *7*(4), 457–472.

Gooley, R., Hogg, C. J., Belov, K., & Grueber, C. E. (2017). No evidence of inbreeding depression in a Tasmanian devil insurance population despite significant variation in inbreeding. *Scientific Reports*, *7*(1), 1830.

Green, R. E., Krause, J., Briggs, A. W., Maricic, T., Stenzel, U., Kircher, M., Patterson, N., Li, H., Zhai, W., Fritz, M. H.-Y., Hansen, N. F., Durand, E. Y., Malaspinas, A.-S., Jensen, J. D., Marques-Bonet, T., Alkan, C., Prüfer, K., Meyer, M., Burbano, H. A., … Pääbo, S. (2010). A draft sequence of the Neandertal genome. *Science*, *328*(5979), 710–722.

Grossen, C., Guillaume, F., Keller, L. F., & Croll, D. (2020). Purging of highly deleterious mutations through severe bottlenecks in Alpine ibex. *Nature Communications*, *11*. https://doi.org/10.1101/605147

Groves, P. (1997). Intraspecific variation in mitochondrial DNA of muskoxen, based on control-region sequences. *Canadian Journal of Zoology*, *75*(4), 568–575.

Gunn, A., & Forchhammer, M. (2022). *Ovibos moschatus.(errata version published in 2016.)*. The IUCN Red List of Threatened Species 2022.

Hanghøj, K., Moltke, I., Andersen, P. A., Manica, A., & Korneliussen, T. S. (2019). Fast and accurate relatedness estimation from high-throughput sequencing data in the presence of inbreeding. *GigaScience*, *8*(5). https://doi.org/10.1093/gigascience/giz034

Hansen, C. C. R., Hvilsom, C., Schmidt, N. M., Aastrup, P., Van Coeverden de Groot, P. J., Siegismund, H. R., & Heller, R. (2018). The Muskox Lost a Substantial Part of Its Genetic Diversity on Its Long Road to Greenland. *Current Biology: CB*, *28*(24), 4022–4028.e5.

Harington, C. R. (1961). *History, distribution and ecology of the Muskoxen*. https://escholarship.mcgill.ca/concern/theses/s7526c702

Hassanin, A., Ropiquet, A., Couloux, A., & Cruaud, C. (2009). Evolution of the mitochondrial genome in mammals living at high altitude: new insights from a study of the tribe Caprini (Bovidae, Antilopinae). *Journal of Molecular Evolution*, *68*(4), 293–310.

Hasselgren, M., Dussex, N., von Seth, J., Angerbjörn, A., Olsen, R.-A., Dalén, L., & Norén, K. (2021). Genomic and fitness consequences of inbreeding in an endangered carnivore. *Molecular Ecology*, *30*(12), 2790–2799.

Jónsson, H., Ginolhac, A., Schubert, M., Johnson, P. L. F., & Orlando, L. (2013). mapDamage2.0: fast approximate Bayesian estimates of ancient DNA damage parameters. *Bioinformatics* , *29*(13), 1682–1684.

Kafle, P., Peller, P., Massolo, A., Hoberg, E., Leclerc, L.-M., Tomaselli, M., & Kutz, S. (2020). Range expansion of muskox lungworms track rapid arctic warming: implications for geographic colonization under climate forcing. In *Scientific Reports* (Vol. 10, Issue 1). https://doi.org/10.1038/s41598-020-74358-5

Kahlke, R.-D. (2014). The origin of Eurasian Mammoth Faunas (Mammuthus–Coelodonta Faunal Complex). *Quaternary Science Reviews*, *96*, 32–49.

Katoh, K., & Standley, D. M. (2013). MAFFT multiple sequence alignment software version 7: improvements in performance and usability. *Molecular Biology and Evolution*, *30*(4), 772–780.

Kearse, M., Moir, R., Wilson, A., Stones-Havas, S., Cheung, M., Sturrock, S., Buxton, S., Cooper, A., Markowitz, S., Duran, C., Thierer, T., Ashton, B., Meintjes, P., & Drummond, A. (2012). Geneious Basic: an integrated and extendable desktop software platform for the organization and analysis of sequence data. *Bioinformatics* , *28*(12), 1647–1649.

Khan, A., Patel, K., Shukla, H., Viswanathan, A., van der Valk, T., Borthakur, U., Nigam, P., Zachariah, A., Jhala, Y. V., Kardos, M., & Ramakrishnan, U. (2021). Genomic evidence for inbreeding depression and purging of deleterious genetic variation in Indian tigers. *Proceedings of the National Academy of Sciences of the United States of America*, *118*(49). https://doi.org/10.1073/pnas.2023018118

Klütsch, C. F. C., Manseau, M., Anderson, M., Sinkins, P., & Wilson, P. J. (2017). Evolutionary reconstruction supports the presence of a Pleistocene Arctic refugium for a large mammal species. *Journal of Biogeography*, *44*(12), 2729–2739.

Knuth, E. (1967). *Archaeology of the Musk-ox Way*. École pratique des hautes études, Sorbonne.

Kolokotronis, S.-O., Macphee, R. D. E., & Greenwood, A. D. (2007). Detection of mitochondrial insertions in the nucleus (NuMts) of Pleistocene and modern muskoxen. *BMC Evolutionary Biology*, *7*, 67.

Korneliussen, T. S., Albrechtsen, A., & Nielsen, R. (2014). ANGSD: Analysis of Next Generation Sequencing Data. *BMC Bioinformatics*, *15*, 356.

Kutschera, V. E., Kierczak, M., van der Valk, T., von Seth, J., Dussex, N., Lord, E., Dehasque, M., Stanton, D. W. G., Khoonsari, P. E., Nystedt, B., Dalén, L., & Díez-del-Molino, D. (2022). GenErode: a bioinformatics pipeline to investigate genome erosion in endangered and extinct species. In *bioRxiv* (p. 2022.03.04.482637). https://doi.org/10.1101/2022.03.04.482637

Kutz, S., Bollinger, T., Branigan, M., Checkley, S., Davison, T., Dumond, M., Elkin, B., Forde, T., Hutchins, W., Niptanatiak, A., & Orsel, K. (2015). Erysipelothrix rhusiopathiae associated with recent widespread muskox mortalities in the Canadian Arctic. *The Canadian Veterinary Journal. La Revue Veterinaire Canadienne*, *56*(6), 560–563.

Kutz, S. J. (2004). "Emerging" Parasitic Infections in Arctic Ungulates. In *Integrative and Comparative Biology* (Vol. 44, Issue 2, pp. 109–118). https://doi.org/10.1093/icb/44.2.109

Kyriazis, C. C., Beichman, A. C., Brzeski, K. E., Hoy, S. R., Peterson, R. O., Vucetich, J. A., Vucetich, L. M., Lohmueller, K. E., & Wayne, R. K. (2022). Genomic underpinnings of population persistence in Isle Royale moose. In *bioRxiv* (p. 2022.04.15.488504). https://doi.org/10.1101/2022.04.15.488504

Kyriazis, C. C., Wayne, R. K., & Lohmueller, K. E. (2021). Strongly deleterious mutations are a primary determinant of extinction risk due to inbreeding depression. *Evolution Letters*, *5*(1), 33–47.

Laikre, L., Ryman, N., & Lundh, N. G. (1997). Estimated inbreeding in a small, wild muskox Ovibos moschatus population and its possible effects on population reproduction. *Biological Conservation*, *79*(2), 197–204.

Lande, R. (1993). Risks of Population Extinction from Demographic and Environmental Stochasticity and Random Catastrophes. *The American Naturalist*, *142*(6), 911–927.

Leigh, J. W., Bryant, D., & Nakagawa, S. (2015). *POPART: full-feature software for haplotype network construction. Methods Ecol. Evol. 6, 1110--1116*.

Lent, P. C. (1998). Alaska's indigenous muskoxen: a history. *Rangelands*, *18*(3-4), 133–144.

Li, H. (2011). A statistical framework for SNP calling, mutation discovery, association mapping and population genetical parameter estimation from sequencing data. *Bioinformatics* , *27*(21), 2987–2993.

Li, H. (2013). Aligning sequence reads, clone sequences and assembly contigs with BWA-MEM. In *arXiv [q-bio.GN]*. arXiv. http://arxiv.org/abs/1303.3997

Li, H., & Durbin, R. (2011). Inference of human population history from individual whole-genome sequences. *Nature, 475*(7357), 493–496.

Li, H., Handsaker, B., Wysoker, A., Fennell, T., Ruan, J., Homer, N., Marth, G., Abecasis, G., Durbin, R., & 1000 Genome Project Data Processing Subgroup. (2009). The Sequence Alignment/Map format and SAMtools. *Bioinformatics* , *25*(16), 2078–2079.

Li, M., Li, X., Wu, Z., Zhang, G., Wang, N., Dou, M., Liu, S., Yang, C., Meng, G., Sun, H. and Hvilsom, C., Xie, G., Li, Y., Li, Z.h., Wang, W., Jiang, Y., Heller, R. & Wang, Y. (2023). Convergent molecular evolution of thermogenesis and circadian rhythm in Arctic ruminants. *Proceedings of the Royal Society B*, 290(1999), p.20230538.

Lord, E., Dussex, N., Kierczak, M., Díez-Del-Molino, D., Ryder, O. A., Stanton, D. W. G., Gilbert, M. T. P., Sánchez-Barreiro, F., Zhang, G., Sinding, M.-H. S., Lorenzen, E. D., Willerslev, E., Protopopov, A., Shidlovskiy, F., Fedorov, S., Bocherens, H., Nathan, S. K. S. S., Goossens, B., van der Plicht, J., … Dalén, L. (2020). Pre-extinction Demographic Stability and Genomic Signatures of Adaptation in the Woolly Rhinoceros. *Current Biology: CB*, *30*(19), 3871–3879.e7.

Lorenzen, E. D., Nogues-Bravo, D., Orlando, L., Weinstock, J., Binladen, J., Marske, K. A., Ugan, A., Borregaard, M. K., Gilbert, M. T. P., Nielsen, R., & Others. (2011). *Species-specific responses of Late Quaternary megafauna to climate and humans. Nature 479, 359e364*.

MacPhee, R. D. E., Tikhonov, A. N., Mol, D., & Greenwood, A. D. (2005). Late Quaternary loss of genetic diversity in muskox (Ovibos). *BMC Evolutionary Biology*, *5*, 49.

Maher, W. J. (1968). Muskox Bone of Possible Wisconsin Age from Banks Island, Northwest Territories. *Arctic*, *21*(4), 260–266.

Maier, R., Flegontov, P., Flegontova, O., Changmai, P., & Reich, D. (2022). On the limits of fitting complex models of population history to genetic data. In *bioRxiv* (p. 2022.05.08.491072). https://doi.org/10.1101/2022.05.08.491072

Marshall, C., & Parson, W. (2021). Interpreting NUMTs in forensic genetics: Seeing the forest for the trees. *Forensic Science International. Genetics, 53*, 102497.

Martin, S. H., & Van Belleghem, S. M. (2017). Exploring Evolutionary Relationships Across the Genome Using Topology Weighting. *Genetics*, *206*(1), 429–438.

Mathur, S., & Andrew DeWoody, J. (2021). Genetic load has potential in large populations but is realized in small inbred populations. In *Evolutionary Applications* (Vol. 14, Issue 6, pp. 1540–1557). https://doi.org/10.1111/eva.13216

Meisner, J., & Albrechtsen, A. (2018). Inferring Population Structure and Admixture Proportions in Low-Depth NGS Data. *Genetics*, *210*(2), 719–731.

Meisner, J., & Albrechtsen, A. (2019). Testing for Hardy–Weinberg equilibrium in structured populations using genotype or low-depth next generation sequencing data. *Molecular Ecology Resources*, *19*(5), 1144–1152.

Meyer, M., & Kircher, M. (2010). Illumina sequencing library preparation for highly multiplexed target capture and sequencing. *Cold Spring Harbor Protocols, 2010*(6), db.

prot5448.

Minh, B. Q., Schmidt, H. A., Chernomor, O., Schrempf, D., Woodhams, M. D., von Haeseler, A., & Lanfear, R. (2020). IQ-TREE 2: New Models and Efficient Methods for Phylogenetic Inference in the Genomic Era. *Molecular Biology and Evolution*, *37*(5), 1530–1534.

Mölder, F., Jablonski, K. P., Letcher, B., Hall, M. B., Tomkins-Tinch, C. H., Sochat, V., Forster, J., Lee, S., Twardziok, S. O., Kanitz, A., Wilm, A., Holtgrewe, M., Rahmann, S., Nahnsen, S., & Köster, J. (2021). Sustainable data analysis with Snakemake. *F1000Research*, *10*, 33.

Mølgaard, H. S. (2002). *Overgrown hooves from Muskoxen (Ovibos moschatus) of Kangaarsuk (Kap Atholl) Northwest Greenland*. Greenland Institute of Natural Resources.

Mooney, J. A., Marsden, C. D., Yohannes, A., Wayne, R. K., & Lohmueller, K. E. (2023). Long-term Small Population Size, Deleterious Variation, and Altitude Adaptation in the Ethiopian Wolf, a Severely Endangered Canid. *Molecular Biology and Evolution*, *40*(1). https://doi.org/10.1093/molbev/msac277

Morin, P. A., Archer, F. I., Avila, C. D., Balacco, J. R., Bukhman, Y. V., Chow, W., Fedrigo, O., Formenti, G., Fronczek, J. A., Fungtammasan, A., Gulland, F. M. D., Haase, B., Peter Heide-Jorgensen, M., Houck, M. L., Howe, K., Misuraca, A. C., Mountcastle, J., Musser, W., Paez, S., … Jarvis, E. D. (2021). Reference genome and demographic history of the most endangered marine mammal, the vaquita. *Molecular Ecology Resources*, *21*(4), 1008–1020.

Mosbacher, J. B., Kristensen, D. K., Michelsen, A., Stelvig, M., & Schmidt, N. M. (2016). Quantifying Muskox Plant Biomass Removal and Spatial Relocation of Nitrogen in a High Arctic Tundra Ecosystem. *Arctic, Antarctic, and Alpine Research*, *48*(2), 229–240.

Mosbacher, J. B., Michelsen, A., Stelvig, M., Hjermstad-Sollerud, H., & Schmidt, N. M. (2019). Muskoxen modify plant abundance, phenology, and nitrogen dynamics in a high arctic fen. *Ecosystems* , *22*(5), 1095–1107.

Nielsen, R., Korneliussen, T., Albrechtsen, A., Li, Y., & Wang, J. (2012). SNP calling, genotype calling, and sample allele frequency estimation from New-Generation Sequencing data. *PloS One*, *7*(7), e37558.

Nursyifa, C., Brüniche-Olsen, A., Garcia-Erill, G., Heller, R., & Albrechtsen, A. (2022). Joint identification of sex and sex-linked scaffolds in non-model organisms using low depth sequencing data. *Molecular Ecology Resources*, *22*(2), 458–467.

Olesen, C. R. (1993). Rapid population increase in an introduced muskox population, West Greenland. *Rangelands*, *13*(1), 27–32.

Orlando, L., Ginolhac, A., Zhang, G., Froese, D., Albrechtsen, A., Stiller, M., Schubert, M., Cappellini, E., Petersen, B., Moltke, I., Johnson, P. L. F., Fumagalli, M., Vilstrup, J. T., Raghavan, M., Korneliussen, T., Malaspinas, A.-S., Vogt, J., Szklarczyk, D., Kelstrup, C. D., … Willerslev, E. (2013). Recalibrating Equus evolution using the genome sequence of an early Middle Pleistocene horse. *Nature*, *499*(7456), 74–78.

Palkopoulou, E., Mallick, S., Skoglund, P., Enk, J., Rohland, N., Li, H., Omrak, A., Vartanyan, S., Poinar, H., Götherström, A., Reich, D., & Dalén, L. (2015). Complete genomes reveal signatures of demographic and genetic declines in the woolly mammoth. *Current Biology: CB*, *25*(10), 1395–1400.

Paradis, E., & Schliep, K. (2019). ape 5.0: an environment for modern phylogenetics and evolutionary analyses in R. *Bioinformatics* , *35*(3), 526–528.

Patterson, N., Moorjani, P., Luo, Y., Mallick, S., Rohland, N., Zhan, Y., Genschoreck, T., Webster, T., & Reich, D. (2012). Ancient Admixture in Human History. *Genetics*, *192*(3), 1065–1093.

Pečnerová, P., Díez-Del-Molino, D., Dussex, N., Feuerborn, T., von Seth, J., van der Plicht, J., Nikolskiy, P., Tikhonov, A., Vartanyan, S., & Dalén, L. (2017). Genome-Based Sexing Provides Clues about Behavior and Social Structure in the Woolly Mammoth. *Current Biology: CB*, *27*(22), 3505–3510.e3.

Pečnerová, P., Díez-Del-Molino, D., Vartanyan, S., & Dalén, L. (2016). Changes in variation at the MHC class II DQA locus during the final demise of the woolly mammoth. *Scientific Reports*, *6*, 25274.

Pečnerová, P., Garcia-Erill, G., Liu, X., Nursyifa, C., Waples, R. K., Santander, C. G., Quinn, L., Frandsen, P., Meisner, J., Stæger, F. F., Rasmussen, M. S., Brüniche-Olsen, A., Hviid Friis Jørgensen, C., da Fonseca, R. R., Siegismund, H. R., Albrechtsen, A., Heller, R., Moltke, I., & Hanghøj, K. (2021). High genetic diversity and low differentiation reflect the ecological versatility of the African leopard. *Current Biology: CB*, *31*(9), 1862–1871.e5.

Pečnerová, P., Palkopoulou, E., Wheat, C. W., Skoglund, P., Vartanyan, S., Tikhonov, A., Nikolskiy, P., van der Plicht, J., Díez-Del-Molino, D., & Dalén, L. (2017). Mitogenome evolution in the last surviving woolly mammoth population reveals neutral and functional consequences of small population size. *Evolution Letters*, *1*(6), 292–303.

Petkova, D., Novembre, J., & Stephens, M. (2016). Visualizing spatial population structure with estimated effective migration surfaces. *Nature Genetics*, *48*(1), 94–100.

Pickrell, J. K., & Pritchard, J. K. (2012). Inference of population splits and mixtures from genome-wide allele frequency data. *PLoS Genetics*, *8*(11), e1002967.

Pimm, S. L., & Raven, P. (2000). Biodiversity. Extinction by numbers [Review of *Biodiversity. Extinction by numbers*]. *Nature*, *403*(6772), 843–845.

Plummer, M., Best, N., Cowles, K., & Vines, K. (2006). CODA: convergence diagnosis and output analysis for MCMC. *R News*, *6*(1), 7–11.

Powers, R. P., & Jetz, W. (2019). Global habitat loss and extinction risk of terrestrial vertebrates under future land-use-change scenarios. *Nature Climate Change*, *9*(4), 323–329.

Prewer, E., Kutz, S., Leclerc, L. M., & Kyle, C. J. (2020). Already at the bottom? Demographic declines are unlikely further to undermine genetic diversity of a large Arctic ungulate: muskox, Ovibos moschatus (Artiodactyla: Bovidae). *Biological Journal of the Linnean Society. Linnean Society of London*, *129*(2), 459–469.

Primmer, C. R. (2009). From conservation genetics to conservation genomics. *Annals of the New York Academy of Sciences*, *1162*, 357–368.

Purcell, S., & Chang, C. (2015). *PLINK 1.9*. www.cog-genomics.org/plink/1.9/

Purvis, A., Gittleman, J. L., Cowlishaw, G., & Mace, G. M. (2000). Predicting extinction risk in declining species. *Proceedings. Biological Sciences / The Royal Society*, *267*(1456), 1947–1952.

Rambaut, A. (2014). *FigTree: Tree figure drawing tool* (Version 1.4.4) [Computer software]. https://github.com/rambaut/figtree

Rambaut, A., Drummond, A. J., Xie, D., Baele, G., & Suchard, M. A. (2018). Posterior Summarization in Bayesian Phylogenetics Using Tracer 1.7. *Systematic Biology*, *67*(5), 901–904.

Ramsey, C. B. (2009). Bayesian Analysis of Radiocarbon Dates. *Radiocarbon*, *51*(1), 337–360.

R Core Team. (2018). *R: A Language and Environment for Statistical Computing*. R Foundation for Statistical Computing. https://www.R-project.org/

Reich, D., Thangaraj, K., Patterson, N., Price, A. L., & Singh, L. (2009). Reconstructing Indian population history. *Nature*, *461*(7263), 489–494.

Reimer, P. J., Austin, W. E. N., Bard, E., Bayliss, A., Blackwell, P. G., Ramsey, C. B., Butzin, M., Cheng, H., Lawrence Edwards, R., Friedrich, M., Grootes, P. M., Guilderson, T. P., Hajdas, I., Heaton, T. J., Hogg, A. G., Hughen, K. A., Kromer, B., Manning, S. W., Muscheler, R., … Talamo, S. (2020). The IntCal20 Northern Hemisphere Radiocarbon Age Calibration Curve (0–55 cal kBP). *Radiocarbon*, *62*(4), 725–757.

Renaud, G., Hanghøj, K., Korneliussen, T. S., Willerslev, E., & Orlando, L. (2019). Joint estimates of heterozygosity and runs of homozygosity for modern and ancient samples. *Genetics*, *212*(3), 587–614.

Robinson, J. A., Brown, C., Kim, B. Y., Lohmueller, K. E., & Wayne, R. K. (2018). Purging of Strongly Deleterious Mutations Explains Long-Term Persistence and Absence of Inbreeding Depression in Island Foxes. *Current Biology: CB*, *28*(21), 3487–3494.e4.

Robinson, J. A., Ortega-Del Vecchyo, D., Fan, Z., Kim, B. Y., vonHoldt, B. M., Marsden, C. D., Lohmueller, K. E., & Wayne, R. K. (2016). Genomic Flatlining in the Endangered Island Fox. *Current Biology: CB*, *26*(9), 1183–1189.

Robinson, J. A., Räikkönen, J., Vucetich, L. M., Vucetich, J. A., Peterson, R. O., Lohmueller, K. E., & Wayne, R. K. (2019). Genomic signatures of extensive inbreeding in Isle Royale wolves, a population on the threshold of extinction. *Science Advances*, *5*(5), eaau0757.

Rstudio Team. (2019). *RStudio: integrated development environment for R*.

Saitou, N., & Nei, M. (1987). The neighbor-joining method: a new method for reconstructing phylogenetic trees. *Molecular Biology and Evolution*, *4*(4), 406–425.

Schliep, K. P. (2011). phangorn: phylogenetic analysis in R. *Bioinformatics* , *27*(4), 592–593.

Schliep, K., Potts, A. J., Morrison, D. A., & Grimm, G. W. (2017). Intertwining phylogenetic trees and networks. *Methods in Ecology and Evolution / British Ecological Society*, *8*(10), 1212–1220.

Schmidt, N. M., Pedersen, S. H., Mosbacher, J. B., & Hansen, L. H. (2015). Long-term patterns of muskox (Ovibos moschatus) demographics in high arctic Greenland. *Polar Biology*, *38*(10), 1667–1675.

Schmidt, N. M., Reneerkens, J., Christensen, J. H., Olesen, M., & Roslin, T. (2019). An ecosystem-wide reproductive failure with more snow in the Arctic. *PLoS Biology*, *17*(10), e3000392.

Schubert, M., Jónsson, H., Chang, D., Der Sarkissian, C., Ermini, L., Ginolhac, A., Albrechtsen, A., Dupanloup, I., Foucal, A., Petersen, B., Fumagalli, M., Raghavan, M., Seguin-Orlando, A., Korneliussen, T. S., Velazquez, A. M. V., Stenderup, J., Hoover, C. A., Rubin, C.-J., Alfarhan, A. H., … Orlando, L. (2014). Prehistoric genomes reveal the genetic foundation and cost of horse domestication. *Proceedings of the National Academy of Sciences of the United States of America*, *111*(52), E5661–E5669.

Schubert, M., Lindgreen, S., & Orlando, L. (2016). AdapterRemoval v2: rapid adapter trimming, identification, and read merging. *BMC Research Notes*, *9*, 88.

Shaffer, M. L. (1981). Minimum Population Sizes for Species Conservation. *Bioscience*, *31*(2), 131–134.

Sinding, M.-H. S., Gopalakrishan, S., Vieira, F. G., Samaniego Castruita, J. A., Raundrup, K., Heide Jørgensen, M. P., Meldgaard, M., Petersen, B., Sicheritz-Ponten, T., Mikkelsen, J. B., Marquard-Petersen, U., Dietz, R., Sonne, C., Dalén, L., Bachmann, L., Wiig, Ø., Hansen, A. J., & Gilbert, M. T. P. (2018). Population genomics of grey wolves and wolf-

like canids in North America. *PLoS Genetics, 14*(11), e1007745.

Skoglund, P., Northoff, B. H., Shunkov, M. V., Derevianko, A. P., Pääbo, S., Krause, J., & Jakobsson, M. (2014). Separating endogenous ancient DNA from modern day contamination in a Siberian Neandertal. *Proceedings of the National Academy of Sciences of the United States of America, 111*(6), 2229–2234.

Skotte, L., Korneliussen, T. S., & Albrechtsen, A. (2013). Estimating individual admixture proportions from next generation sequencing data. *Genetics, 195*(3), 693–702.

Smit, A. F. A., Hubley, R., & Green, P. (2019). *2013--2015. RepeatMasker Open-4.0.*

Smit, A., & Hubley, R. (2017). RMBlast. *Seattle, WA: Institute for Systems Biology. [cited 2017 Dec 15] Available from: Http://www. Repeatmasker. org/RMBlast. Html.*

Soule, M. E. (1976). Allozyme variation, its determinats in space and time. *Moleculor Evolution*, 60–77.

Stecher, G., Tamura, K., & Kumar, S. (2020). Molecular Evolutionary Genetics Analysis (MEGA) for macOS. *Molecular Biology and Evolution, 37*(4), 1237–1239.

Steiner, C. C., Putnam, A. S., Hoeck, P. E. A., & Ryder, O. A. (2013). Conservation genomics of threatened animal species. *Annual Review of Animal Biosciences, 1*, 261–281.

Stoffel, M. A., Johnston, S. E., Pilkington, J. G., & Pemberton, J. M. (2021). Genetic architecture and lifetime dynamics of inbreeding depression in a wild mammal. *Nature Communciations, 12*(2972). https://doi.org/10.1101/2020.05.27.118877

Stokes, C. R. (2017). Deglaciation of the Laurentide Ice Sheet from the Last Glacial Maximum. *Cuadernos de Investigación Geográfica., 43*(2), 0.

Taylor, R. S., Manseau, M., Klütsch, C. F. C., Polfus, J. L., Steedman, A., Hervieux, D., Kelly, A., Larter, N. C., Gamberg, M., Schwantje, H., & Wilson, P. J. (2021). Population dynamics of caribou shaped by glacial cycles before the last glacial maximum. *Molecular Ecology, 30*(23), 6121–6143.

Tener, J. S. (1965). *Muskoxen in Canada: A Biological and Taxonomic Review*. Department of Northern Affairs and National Resources, Canadian Wildlife Service.

Thomas, J. E., Carvalho, G. R., Haile, J., Rawlence, N. J., Martin, M. D., Ho, S. Y., Sigfússon, A. Þ., Jósefsson, V. A., Frederiksen, M., Linnebjerg, J. F., Samaniego Castruita, J. A., Niemann, J., Sinding, M.-H. S., Sandoval-Velasco, M., Soares, A. E., Lacy, R., Barilaro, C., Best, J., Brandis, D., … Knapp, M. (2019). Demographic reconstruction from ancient DNA supports rapid extinction of the great auk. *eLife, 8*. https://doi.org/10.7554/eLife.47509

Thulin, C.-G., Englund, L., Ericsson, G., & Spong, G. (2011). The impact of founder events and introductions on genetic variation in the muskox Ovibos moschatus in Sweden. In *Acta Theriologica* (Vol. 56, Issue 4, pp. 305–314). https://doi.org/10.1007/s13364-011-0035-z

Tomaselli, M., Dalton, C., Duignan, P. J., Kutz, S., van der Meer, F., Kafle, P., Surujballi, O., Turcotte, C., & Checkley, S. (2016). Contagious Ecthyma, Rangiferine Brucellosis, and Lungworm Infection in a Muskox (*Ovibos moschatus*) from the Canadian Arctic, 2014. In *Journal of Wildlife Diseases* (Vol. 52, Issue 3, pp. 719–724). https://doi.org/10.7589/2015-12-327

To, T.-H., Jung, M., Lycett, S., & Gascuel, O. (2016). Fast Dating Using Least-Squares Criteria and Algorithms. *Systematic Biology, 65*(1), 82–97.

van der Valk, T., de Manuel, M., Marques-Bonet, T., & Guschanski, K. (2021). Estimates of genetic load suggest frequent purging of deleterious alleles in small populations. In *bioRxiv* (p. 696831). https://doi.org/10.1101/696831

van der Valk, T., Díez-Del-Molino, D., Marques-Bonet, T., Guschanski, K., & Dalén, L. (2019). Historical Genomes Reveal the Genomic Consequences of Recent Population Decline in Eastern Gorillas. *Current Biology: CB*, *29*(1), 165–170.e6.

Van Coeverden de Groot, P. J. V. C. (2001). *Conservation genetic implications of microsatellite variation in the muskox Ovibos moschatus: the effect of refugial isolation and the Arctic Ocean on genetic structure*. Queen's University.

Van Rossum, G., & Drake, F. L. (2009). *Python 3 Reference Manual: (Python Documentation Manual Part 2)*. CreateSpace Independent Publishing Platform.

Vibe, C. (1958). *The musk ox in East Greenland*. *22*(1-4), 168–174.

Waltari, E., & Cook, J. A. (2005). Hares on ice: phylogeography and historical demographics of Lepus arcticus, L. othus, and L. timidus (Mammalia: Lagomorpha). *Molecular Ecology*, *14*(10), 3005–3016.

Waples, R. K., Albrechtsen, A., & Moltke, I. (2019). Allele frequency-free inference of close familial relationships from genotypes or low-depth sequencing data. *Molecular Ecology*, *28*(1), 35–48.

Westbury, M. V., Hartmann, S., Barlow, A., Wiesel, I., Leo, V., Welch, R., Parker, D. M., Sicks, F., Ludwig, A., Dalén, L., & Hofreiter, M. (2018). Extended and Continuous Decline in Effective Population Size Results in Low Genomic Diversity in the World's Rarest Hyena Species, the Brown Hyena. In *Molecular Biology and Evolution* (Vol. 35, Issue 5, pp. 1225–1237). https://doi.org/10.1093/molbev/msy037

Westbury, M. V., Petersen, B., Garde, E., Heide-Jørgensen, M. P., & Lorenzen, E. D. (2019). Narwhal Genome Reveals Long-Term Low Genetic Diversity despite Current Large Abundance Size. *iScience*, *15*, 592–599.

Wickham, H. (2021). ggplot2: elegant graphics for data analysis. 2016. *https://ggplot2. Tidyverse. Org. Doi*, *10*, 978–973.

Xue, Y., Prado-Martinez, J., Sudmant, P. H., Narasimhan, V., Ayub, Q., Szpak, M., Frandsen, P., Chen, Y., Yngvadottir, B., Cooper, D. N., de Manuel, M., Hernandez-Rodriguez, J., Lobon, I., Siegismund, H. R., Pagani, L., Quail, M. A., Hvilsom, C., Mudakikwa, A., Eichler, E. E., … Scally, A. (2015). Mountain gorilla genomes reveal the impact of long-term population decline and inbreeding. *Science*, *348*(6231), 242–245.

Yang, D. Y., Eng, B., Waye, J. S., Dudar, J. C., & Saunders, S. R. (1998). *Technical Note : Improved DNA Extraction From Ancient Bones Using Silica-Based Spin Columns*. *543*(December 1997), 539–543.

Zhou, X., Sun, F., Xu, S., Fan, G., Zhu, K., Liu, X., Chen, Y., Shi, C., Yang, Y., Huang, Z., Chen, J., Hou, H., Guo, X., Chen, W., Chen, Y., Wang, X., Lv, T., Yang, D., Zhou, J., … Yang, G. (2013). Baiji genomes reveal low genetic variability and new insights into secondary aquatic adaptations. *Nature Communications, 4*, 2708.

Data Accessibility Statement

Raw sequence reads are deposited in the European Nucleotide Archive under study accession ID: PRJEB64293.

Conflict of Interest Statement

The authors declare no conflict of interest.

Author contributions

H.S. and R.H. conceived the project. P.P., H.S., R.H., I.M., A.A., E.L., L.D. designed the study. C.H. and S.L. provided the muskox reference genome. N.M.S., L.D., C.C., F.D., J.Må., M.H.S.S., A.G., M.P.H.-J., S.V. and C.H. collected or provided the samples. E.L. performed laboratory work on the ancient sample. A.A-C. and L.R. performed laboratory work on the modern samples. P.P. processed, mapped, and filtered the sequencing data from the modern samples. E.L. processed, mapped, and filtered the sequencing data from the ancient sample. P.P. computed the genotype likelihoods and genotype calls, performed analyses of populations structure, connectivity, demography, genetic diversity, inbreeding, and mitochondrial phylogeny and dating. E.L. performed the estimation of nuclear divergence times, and analyses of genetic load. G.G.E. performed analyses of D-statistics and qpGraph. M.S.R. performed the TreeMix analysis. K.H., G.G.E, X.L., C.G.S., J.M., M.R.S., T.v.d.V., A.A., R.H., I.M. provided scripts and advice for the bioinformatic analyses. N.M.S., K.R., and L.D. provided advice on biological interpretations. P.P. wrote the manuscript together with E.L. and with the help of all co-authors.
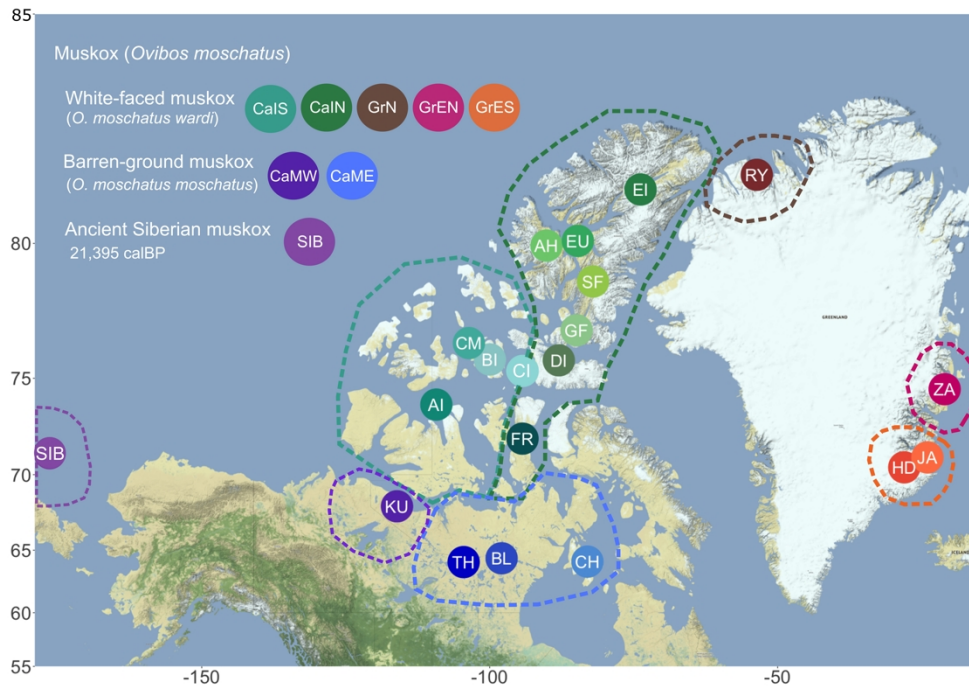
Figure 1. A map showing the sampled regions (dashed lines) and locations (smaller points), based on the genetic groupings determined in this study.
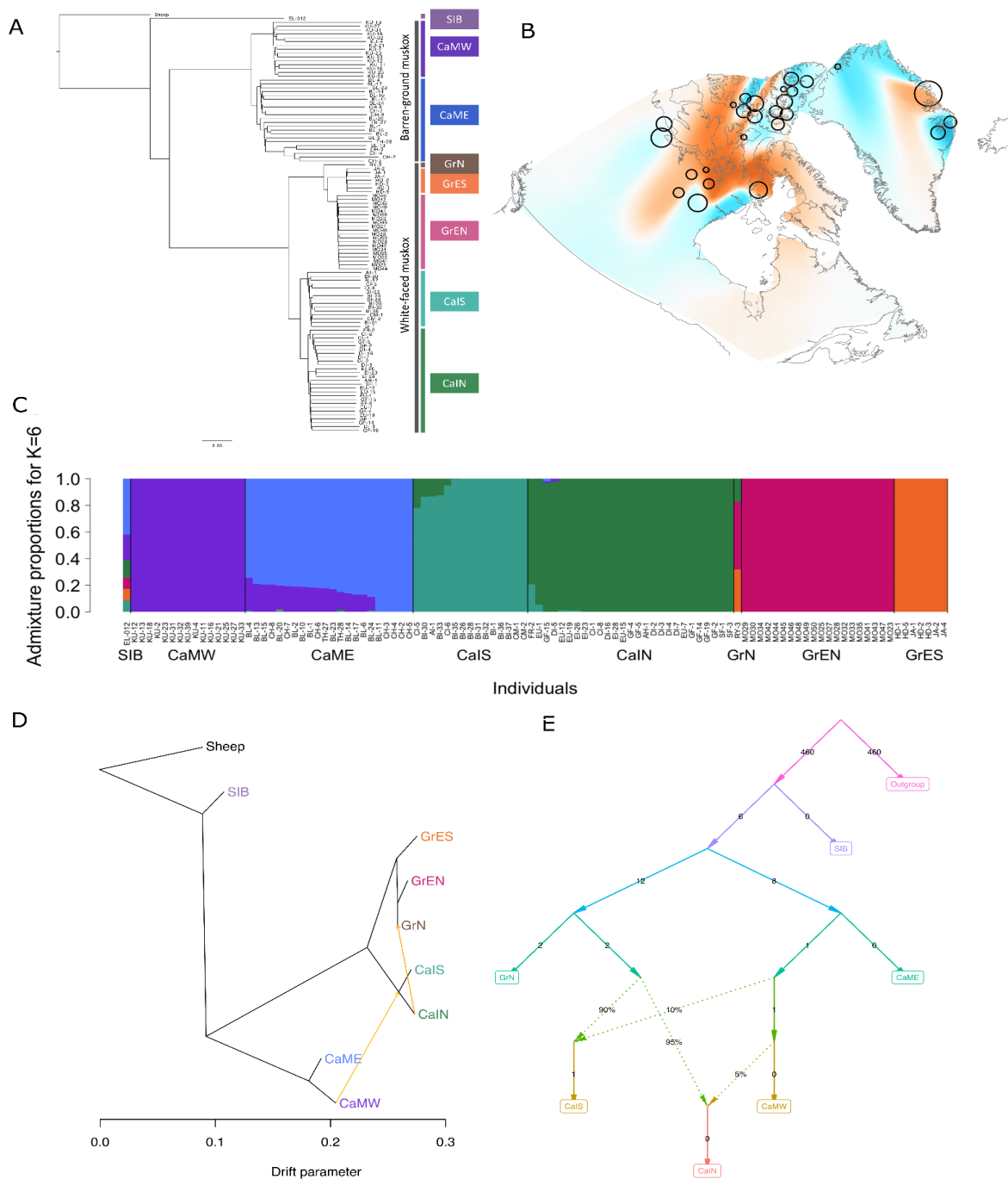
Figure 2. Population structure of muskox. A) A Neighbor-Joining tree of genetic distances based on an IBS matrix. B) EEMS analysis reveals the areas of relative genetic connectivity (blue) and barriers to gene flow (orange). C) A plot of admixture proportions at K=6 inferred using ngsAdmix. D) TreeMix with two migration edges supporting gene flow from the Canadian mainland to the Canadian islands, as well as from the northern Canadian islands to northern Greenland. E) qpGraph with two migration events (GrEN and GrES were removed for this analysis as the low variation does not offer enough information).
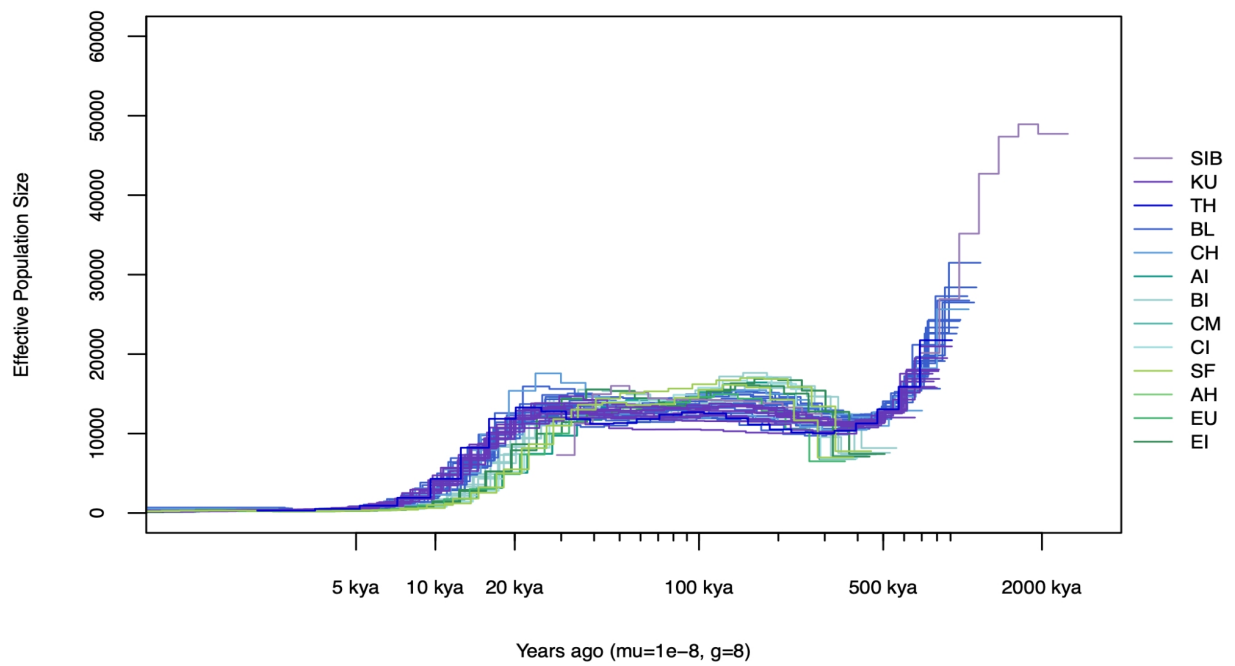
Figure 3. Reconstruction of effective population size through time in PSMC, using the ancient Siberian muskox and the high-depth genomes of present-day Canadian muskoxen. Greenlandic muskoxen were not included due to low heterozygosity biasing the results.
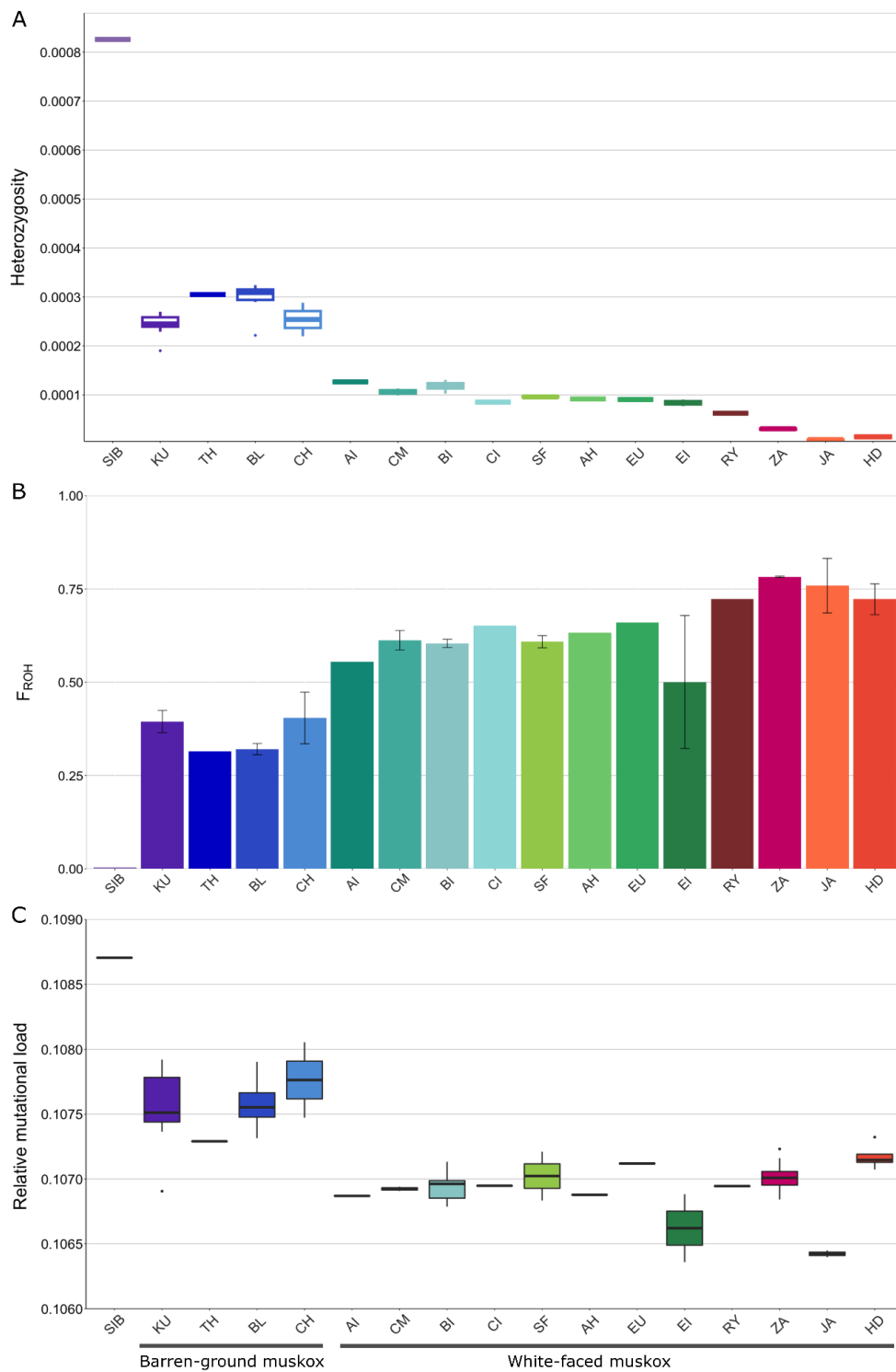
Figure 4. Genetic diversity, inbreeding coefficients, and genetic load. A) Genome-wide heterozygosity estimates based on genotype calls (Table S4). See also the log10-scale version in Figure S17 and estimates from 1dSFS, with and without transitions, in Figure S18. B) F_{ROH} measured in PLINK as the proportion of the genome in ROH of at least 1 MB. Error bars represent standard error. C) Relative mutational load estimated using GERP on 1,746,415 sites and allowing missingness of up to 10%. For reference on locations see Figure 1.
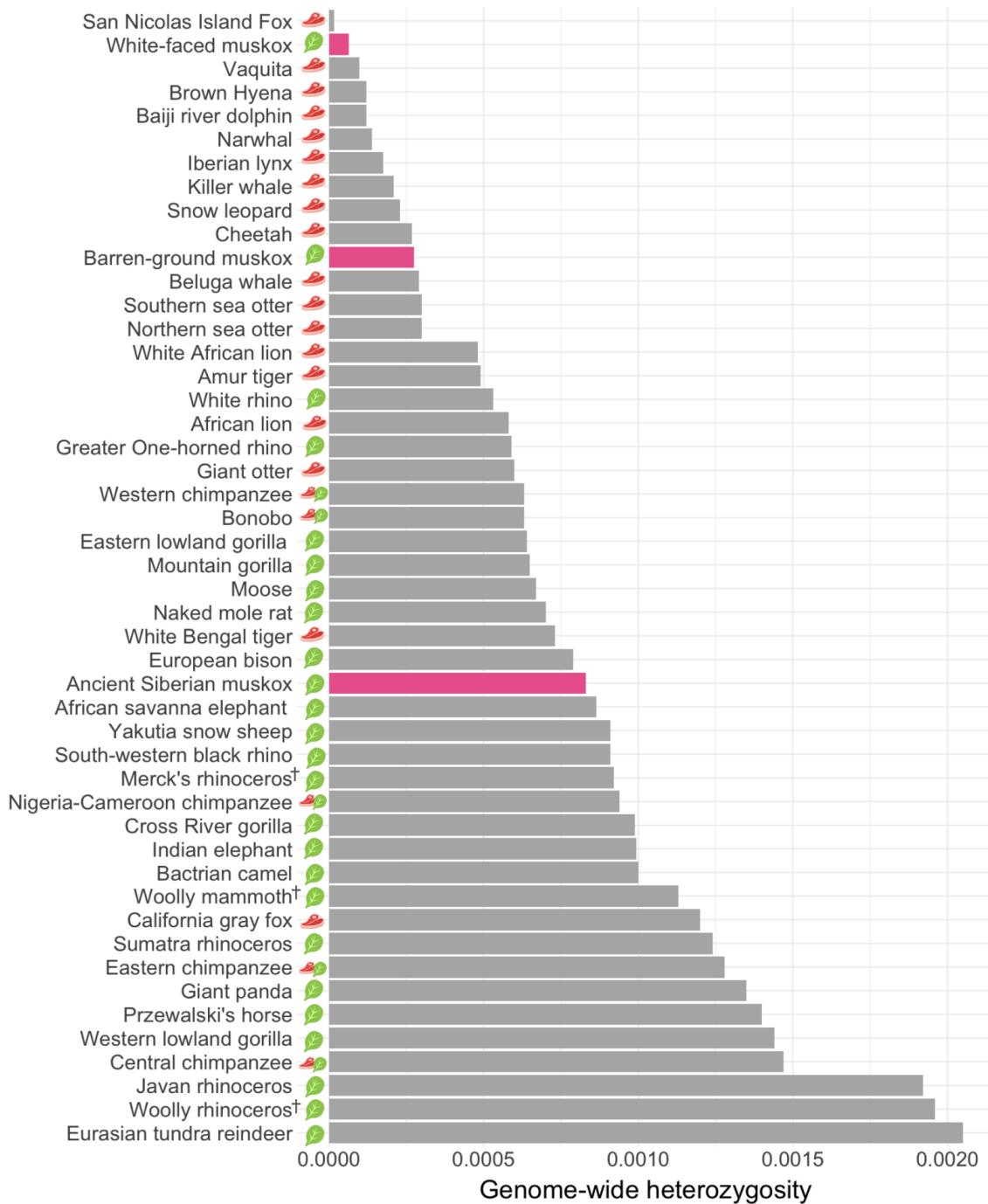
Figure 5. Comparison of the genome-wide heterozygosity in the two muskox subspecies, the ancient Siberian muskox, and a range of previously published estimates (Table S7) in red-listed mammal taxa at the lower end of the heterozygosity spectrum. It should be noted that this comparison is approximate as the estimates are influenced by the used pipelines and filtering criteria. Extinct species are indicated with a cross. Icons were obtained from icons8.com.

Figure 6. The distribution of heterozygous (pink) and homozygous (grey) sites along the largest scaffold (scaf10) illustrates the relative proportions of the scaffold found in ROH and depleted of genetic variation for one randomly selected high depth genome for each population.
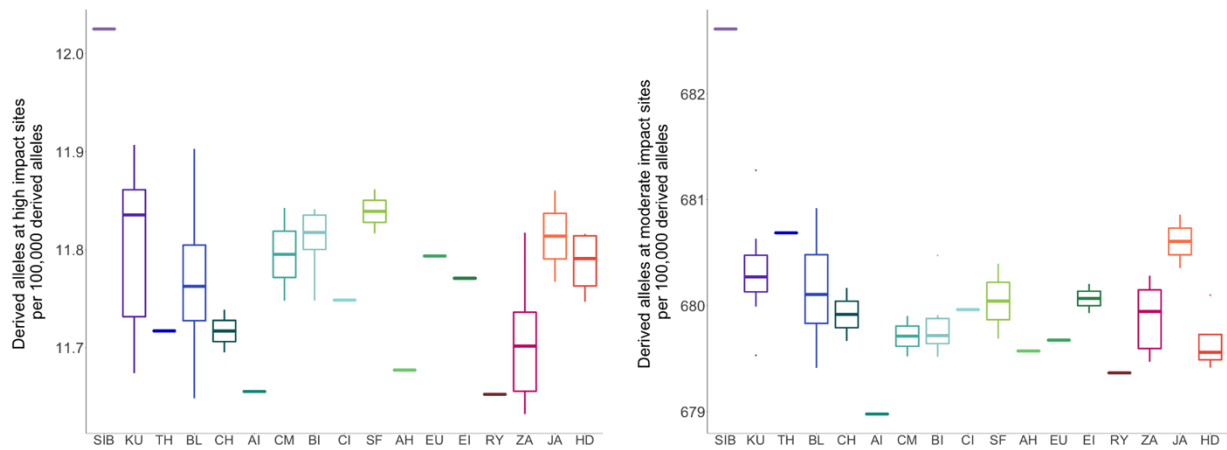
Figure 7. Total mutational load estimated as the number of derived alleles in a functional impact category per 100,000 derived alleles. High impact category corresponds to loss-of-function mutations. and moderate-impact category represents missense mutations. For reference on locations see Figure 1.